



ADVCOMP 2018

The Twelfth International Conference on Advanced Engineering Computing and
Applications in Sciences

ISBN: 978-1-61208-677-4

November 18 - 22, 2018

Athens, Greece

ADVCOMP 2018 Editors

Claus-Peter Rückemann, Leibniz Universität Hannover / Westfälische
Wilhelms-Universität Münster / North-German Supercomputing Alliance
(HLRN), Germany

Ahmad Rafi Qawasmeh, The Hashemite University, Jordan

ADVCOMP 2018

Forward

The Twelfth International Conference on Advanced Engineering Computing and Applications in Sciences (ADVCOMP 2018), held between November 18, 2018 and November 22, 2018 in Athens, Greece, continued a series of events meant to bring together researchers from the academia and practitioners from the industry in order to address fundamentals of advanced scientific computing and specific mechanisms and algorithms for particular sciences.

With the advent of high performance computing environments, virtualization, distributed and parallel computing, as well as the increasing memory, storage and computational power, processing particularly complex scientific applications and voluminous data is more affordable. With the current computing software, hardware and distributed platforms effective use of advanced computing techniques is more achievable.

The conference provided a forum where researchers were able to present recent research results and new research problems and directions related to them. The conference sought contributions presenting novel research in all aspects of new scientific methods for computing and hybrid methods for computing optimization, as well as advanced algorithms and computational procedures, software and hardware solutions dealing with specific domains of science.

The conference had the following tracks:

- Computing applications in science
- Computing mechanisms and methods
- Multidisciplinary Mobile and Web Applications in Modern Life

We take here the opportunity to warmly thank all the members of the ADVCOMP 2018 technical program committee, as well as all the reviewers. The creation of such a high quality conference program would not have been possible without their involvement. We also kindly thank all the authors that dedicated much of their time and effort to contribute to ADVCOMP 2018. We truly believe that, thanks to all these efforts, the final conference program consisted of top quality contributions.

We also gratefully thank the members of the ADVCOMP 2018 organizing committee for their help in handling the logistics and for their work that made this professional meeting a success.

We hope that ADVCOMP 2018 was a successful international forum for the exchange of ideas and results between academia and industry and to promote further progress in the field of engineering computing and applications in sciences. We also hope that Athens, Greece, provided a pleasant environment during the conference and everyone saved some time to enjoy the historic charm of the city.

ADVCOMP 2018 Chairs

ADVCOMP Steering Committee

Juha Röning, University of Oulu, Finland
Paul Humphreys, Ulster University, UK
Wasif Afzal, Mälardalen University, Sweden
Hans-Joachim Bungartz, TUM, Germany
Andreas Rausch, Technische Universität Clausthal, Germany
Ivan Rodero, Rutgers University - Piscataway, USA
Dean Vucinic, Vrije Universiteit Brussel (VUB), Belgium | FERIT, Croatia,
Wenbing Zhao, Cleveland State University, USA
Rudolf Berrendorf, Bonn-Rhein-Sieg University, Germany

ADVCOMP Industry/Research Advisory Committee

Yuri Alexeev, Argonne National Laboratory, USA
Marcin Hojny, AGH University of Science and Technology, Kraków, Poland
Alice Koniges, Lawrence Berkeley Laboratory/NERSC, USA
Marcin Paprzycki, Systems Research Institute, Polish Academy of Sciences, Poland
Folker Meyer, Argonne National Laboratory Computation Institute and Medical School |
University of Chicago, USA
Jian Lin, Huawei Technologies Co. Ltd, Hangzhou, China
Simon Tsang, Vencore Labs Inc., USA
Alfred Geiger, T-Systems Solutions for Research GmbH, Germany
Hugo Daniel Meyer, University of Amsterdam, Netherlands

ADVCOMP 2018 Committee

ADVCOMP Steering Committee

Juha Röning, University of Oulu, Finland
Paul Humphreys, Ulster University, UK
Wasif Afzal, Mälardalen University, Sweden
Hans-Joachim Bungartz, TUM, Germany
Andreas Rausch, Technische Universität Clausthal, Germany
Ivan Rodero, Rutgers University - Piscataway, USA
Dean Vucinic, Vrije Universiteit Brussel (VUB), Belgium | FERIT, Croatia,
Wenbing Zhao, Cleveland State University, USA
Rudolf Berrendorf, Bonn-Rhein-Sieg University, Germany

ADVCOMP Industry/Research Advisory Committee

Yuri Alexeev, Argonne National Laboratory, USA
Marcin Hojny, AGH University of Science and Technology, Kraków, Poland
Alice Koniges, Lawrence Berkeley Laboratory/NERSC, USA
Marcin Paprzycki, Systems Research Institute, Polish Academy of Sciences, Poland
Folker Meyer, Argonne National Laboratory Computation Institute and Medical School |
University of Chicago, USA
Jian Lin, Huawei Technologies Co. Ltd, Hangzhou, China
Simon Tsang, Vencore Labs Inc., USA
Alfred Geiger, T-Systems Solutions for Research GmbH, Germany
Hugo Daniel Meyer, University of Amsterdam, Netherlands

ADVCOMP 2018 Technical Program Committee

Waleed H. Abdulla, University of Auckland, New Zealand
Mohamed Riduan Abid, Alakhawayn University, Morocco
Wasif Afzal, Mälardalen University, Sweden
Ayaz Ahmad, COMSATS Institute of Information Technology, Pakistan
Francisco Airton Silva, Federal University of Piauí, Brazil
Yuri Alexeev, Argonne National Laboratory, USA
Sónia Maria Almeida da Luz, Polytechnic Institute of Leiria, Portugal
Daniel Andresen, Kansas State University, USA
Omar Andres Carmona Cortes, Instituto Federal do Maranhão, Brazil
Alberto Antonietti, Politecnico di Milano, Italy
Ehsan Atoofian, Lakehead University, Canada
Abdel-Hameed Badawy, New Mexico State University & Los Alamos National Laboratory, USA
Doo-Hwan Bae, School of Computing - KAIST, Korea

Jorge Barbosa, Universidade do Porto, Portugal
Carlos Becker Westphall, University of Santa Catarina, Brazil
R. Ben Djemaa, Institut Supérieur d'Informatique et des Techniques de Communication,
Tunisia
Rudolf Berrendorf, Bonn-Rhein-Sieg University, Germany
Md Zakirul Alam Bhuiyan, Fordham University, USA
Tekin Bicer, Argonne National Laboratory, USA
Muhammad Naufal Bin Mansor, University Malaysia Perlis, Malaysia
Kai Bu, Zhejiang University, China
Pedro H. Bugatti, Federal University of Technology - Paraná (UTFPR), Brazil
Hans-Joachim Bungartz, TUM, Germany
Maxwell Cai, Leiden University, Netherlands
Xiao-Chuan Cai, University of Colorado Boulder, USA
Laura Carrington, PMAc Labs - SDSC/UCSD / EP Analytic Inc., USA
Metec Celik, Erciyes University, Turkey
Hsi-Ya Chang, National Center for High-performance Computing, Taiwan
Huangke Chen, National University of Defense Technology, China
Liang Chen, University of West London, UK
Christian Contarino, University of Trento, Italy
Juan Manuel Corchado Rodríguez, University of Salamanca, Spain
Andrews Cordolino Sobral, University of La Rochelle, France
Gianpiero Costantino, IIT - CNR, Italy
Subhro Das, IBM T.J. Watson Research Center, New York, USA
Marisa da Silva Maximiano, Polytechnic of Leiria, Portugal
Marcelo de Paiva Guimarães, Federal University of São Paulo, Brazil
Vassilios V. Dimakopoulos, University of Ioannina, Greece
Mohammed Nabil El Korso, Paris X University, France
Maha Elarbi, University of Tunis (ISG-Campus), Tunisia
Mahdi Esfahanian, Florida Atlantic University, USA
Javier Fabra, Universidad de Zaragoza, Spain
Tiziano Fagni, Institute of Informatics and Telematics (IIT) - CNR, Pisa, Italy
Ali Farhadi, University of Memphis, USA
Akemi Galvez Tomida, University of Cantabria, Spain
Marc Gamell, Intel Corporation, USA
Félix J. García Clemente, University of Murcia, Spain
Leonardo Garrido, Tecnológico de Monterrey, Mexico
Filippo Gaudenzi, Università degli Studi di Milano, Italy
Alfred Geiger, T-Systems Solutions for Research GmbH, Germany
Mahsa Ghasemi, The University of Texas at Austin, USA
J. Paul Gibson, Telecom Sud Paris, France
Jing Gong, KTH Royal Institute of Technology, Sweden
Teofilo Gonzalez, University of California Santa Barbara, USA
Bernard Grabot, LGP-ENIT, France
Jerzy Grzymala-Busse, University of Kansas, USA

Jagadeesh Gunda, University of Edinburgh, UK
Yanfei Guo, MCS Division | ANL, USA
Maki Habib, American University in Cairo, Egypt
Shaza Hanif, Higher Colleges of Technology, Sharjah, United Arab Emirates
Abolfazl Hashemi, University of Texas at Austin, USA
Houcine Hassan, Universidad Politécnica de Valencia, Spain
Mohd Helmy Abd Wahab, Universiti Tun Hussein Onn Malaysia, Malaysia
Marcin Hojny, AGH University of Science and Technology, Kraków, Poland
Wladyslaw Homenda, Warsaw University of Technology, Poland
Tzung-Pei Hong, National University of Kaohsiung, Taiwan
Michael Hübner, Ruhr-University of Bochum, Germany
Paul Humphreys, Ulster University, UK
Andres Iglesias, University of Cantabria, Spain / Toho University, Japan
Hiroshi Ishikawa, Tokyo Metropolitan University, Japan
Mohamed Ismail, University of Regina, Canada
Koteswar Rao Jerripothula, Nanyang Technological University, Singapore
Yiming Ji, University of South Carolina Beaufort, USA
Eugene John, The University of Texas at San Antonio, USA
Kyungtae Kang, Hanyang University, Korea
Attila Kertesz, University of Szeged, Hungary
Jie Kong, Xi'an Shiyou University, China
Alice Koniges, Lawrence Berkeley Laboratory/NERSC, USA
Harald Köstler, Friedrich-Alexander University Erlangen-Nürnberg, Germany
Leszek Koszalka, Wroclaw University of Science and Technology, Poland
Pan Lai, Nanyang Technological University, Singapore
Seyong Lee, Oak Ridge National Laboratory, USA
Maurizio Leotta, University of Genova, Italy
Clement Leung, Hong Kong Baptist University - United International College, Hong Kong
Yiu-Wing Leung, Hong Kong Baptist University, Kowloon Tong, Hong Kong
Jiajia Li, Georgia Institute of Technology, USA
Jian Li, University of Massachusetts Amherst, USA
Yiheng Liang, Bridgewater State University, USA
Jian Lin, Huawei Technologies Co. Ltd, Hangzhou, China
Chin-Jung Liu, Michigan State University, USA
Xiaoyi Lu, The Ohio State University, USA
Glenn Luecke, Iowa State University, USA
Emilio Luque, University Autònoma of Barcelona (UAB), Spain
Stephane Maag, Telecom SudParis, France
Elbert E. N. Macau, Instituto Nacional de Pesquisas Espaciais – INPE, Brazil
Frederic Magoules, CentraleSupélec | Université Paris-Saclay, France
Parikshit Maini, IIT-Delhi, India
Shikharesh Majumdar, Carleton University, Canada
Laci Mary Manhães, Public University of Navarre, Spain
Claudia Marcos, ISISTAN Research Institute | UNICEN University, Argentina

Marcin Markowski, Wroclaw University of Science and Technology, Poland
Alessandro Margara, Politecnico di Milano, Italy
Cleyton Mário de Oliveira Rodrigues, University of Pernambuco, Brazil
Piyush Mehrotra, NASA Ames Research Center, USA
Gabriele Mencagli, University of Pisa, Italy
Folker Meyer, Argonne National Laboratory Computation Institute and Medical School |
University of Chicago, USA
Hugo Daniel Meyer, University of Amsterdam, Netherlands
Mariofanna Milanova, University of Arkansas at Little Rock, USA
Subrata Mitra, Adobe Research, India
Ilya Moiseenko, Cisco Systems, USA
Sébastien Monnet, University Savoie Mont Blanc, France
Vadim Mottl, Computing Center of the Russian Academy of Sciences / Moscow Institute of
Physics and Technology, Russia
Laurent Nana, Université de Bretagne Occidentale, France
Elena Maria Navarro Martinez, Universidad de Castilla-La Mancha, Spain
Sarah Odofin, Northumbria University, UK
Joanna Isabelle Olszewska, University of West Scotland, UK
Marcin Paprzycki, Systems Research Institute, Polish Academy of Sciences, Poland
Prantosh Kumar Paul, Raiganj University, West Bengal, India
Agostino Poggi, Università degli Studi di Parma, Italy
Swaroop Pophale, Oak Ridge National Laboratory, USA
Sumit Purohit, Pacific Northwest National Laboratory, USA
Ahmad Rafi Qawasmeh, The Hashemite University, Jordan
Andreas Rausch, Technische Universität Clausthal, Germany
Diego P. Ruiz, University of Granada, Spain
Kwangjin Park, Wonkwang University, South Korea
Sonia Pérez Díaz, University of Alcalá, Spain
Radu-Emil Precup, Politehnica University of Timisoara, Romania
Shuhui Qu, Center for Sustainable Development and Global Competitiveness -Stanford
University, USA
Vaibhav Rastogi, University of Wisconsin, USA
Javed Razzaq, Bonn-Rhein-Sieg University of Applied Sciences, Germany
Barbara Re, University of Camerino, Italy
Carlos Reaño, Technical University of Valencia, Spain
Michele Risi, University of Salerno, Italy
Ivan Rodero, Rutgers University - Piscataway, USA
Juha Röning, University of Oulu, Finland
Swarup Roy, North-Eastern Hill University, India
Julio Sahuquillo, Universitat Politecnica de Valencia, Spain
Subhash Saini, NASA, USA
Sebastiano Fabio Schifano, Università di Ferrara, Italy
Erich Schweighofer, University of Vienna, Austria
Wael Sellami, University of Monastir, Tunisia

Alireza Shahrabi, Glasgow Caledonian University, UK
Justin Y. Shi, Temple University, USA
Neha Shreya, Indian Institute of Tourism and Travel management, Noida, India
Min Si, Argonne National Laboratory, USA
Sören Sonntag, Intel, Germany
Francesco Spegni, Università Politecnica delle Marche, Italy
Giandomenico Spezzano, ICAR-CNR | University of Calabria, Italy
Emanuele Storti, Università Politecnica delle Marche, Italy
Yulei Sui, University of New South Wales (UNSW), Australia
Yifan Sun, Technicolor Research, Los Altos, California
Andrei Tchernykh, CICESE Research Center, Mexico
Priscila Tiemi Maeda Saito, Federal University of Technology - Paraná (UTFPR-CP), Brazil
Jesmin Jahan Tithi, Intel Corp., USA
QuocNam Tran, The University of South Dakota, USA
Simon Tsang, Vencore Labs Inc., USA
Costas Vassilakis, University of the Peloponnese, Greece
Adriano Velasque Werhli, Universidade Federal do Rio Grande - FURG, Brazil
Juan Vicente Capella Hernández, Universitat Politècnica de València, Spain
Dario Vieira, EFREI, France
Konstantinos Votis, Information Technologies Institute | Centre for Research and Technology Hellas, Thessaloniki, Greece
Dean Vucinic, Vrije Universiteit Brussel (VUB), Belgium | FERIT, Croatia
Guodong Wang, South Dakota School of Mines and Technology, USA
Yanshan Wang, Mayo Clinic, Rochester, USA
Yunsheng Wang, Kettering University, USA
Xianglin Wei, Nanjing Telecommunication Technology Research Institute, China
Gabriel Wittum, Goethe University Frankfurt, Germany
Hui Wu, The University of New South Wales, Australia
Mudasser F. Wyne, National University, USA
Qiao Xiang, Yale University, USA
Cong-Cong Xing, Nicholls State University, USA
Zhijie Xu, University of Huddersfield, UK
Reda Yaich, Institut Mines-Télécom, France
Xu Yang, Illinois Institute of Technology, Chicago, USA
Yingzhen Yang, Snap Research, Australia
Xiaodong Yu, Virginia Tech, USA
Quan Yuan, University of Texas of the Permian Basin, USA
Michael Zapf, University of Applied Sciences Nuremberg, Germany
Vesna Zeljkovic, Lincoln University, USA
Jianping Zeng, University of Nebraska-Lincoln, USA
Ruochen Zeng, Marvell Semiconductor, USA
Na Zhang, VMware Inc., USA
Wenbing Zhao, Cleveland State University, USA

Copyright Information

For your reference, this is the text governing the copyright release for material published by IARIA.

The copyright release is a transfer of publication rights, which allows IARIA and its partners to drive the dissemination of the published material. This allows IARIA to give articles increased visibility via distribution, inclusion in libraries, and arrangements for submission to indexes.

I, the undersigned, declare that the article is original, and that I represent the authors of this article in the copyright release matters. If this work has been done as work-for-hire, I have obtained all necessary clearances to execute a copyright release. I hereby irrevocably transfer exclusive copyright for this material to IARIA. I give IARIA permission to reproduce the work in any media format such as, but not limited to, print, digital, or electronic. I give IARIA permission to distribute the materials without restriction to any institutions or individuals. I give IARIA permission to submit the work for inclusion in article repositories as IARIA sees fit.

I, the undersigned, declare that to the best of my knowledge, the article does not contain libelous or otherwise unlawful contents or invading the right of privacy or infringing on a proprietary right.

Following the copyright release, any circulated version of the article must bear the copyright notice and any header and footer information that IARIA applies to the published article.

IARIA grants royalty-free permission to the authors to disseminate the work, under the above provisions, for any academic, commercial, or industrial use. IARIA grants royalty-free permission to any individuals or institutions to make the article available electronically, online, or in print.

IARIA acknowledges that rights to any algorithm, process, procedure, apparatus, or articles of manufacture remain with the authors and their employers.

I, the undersigned, understand that IARIA will not be liable, in contract, tort (including, without limitation, negligence), pre-contract or other representations (other than fraudulent misrepresentations) or otherwise in connection with the publication of my work.

Exception to the above is made for work-for-hire performed while employed by the government. In that case, copyright to the material remains with the said government. The rightful owners (authors and government entity) grant unlimited and unrestricted permission to IARIA, IARIA's contractors, and IARIA's partners to further distribute the work.

Table of Contents

Time Series Forecasting using ARIMA Model A Case Study of Mining Face Drilling Rig <i>Hussan Al-Chalabi, Yamur Al-Douri, and Jan Lundberg</i>	1
Time Series Forecasting using Genetic Algorithm: A Case Study of Maintenance Cost Data for Tunnel Fans <i>Yamur Al Douri, Hussan Al-Chalabi, and Jan Lundberg</i>	4
Hierarchical Multiscale Computational Methodologies for the Study of Complex Molecular Systems <i>Georgios Kritikos, Anthony Chazirakis, Petra Bacova, Anastassia N. Rissanou, Evangelia Kalligiannaki, and Vagelis Harmandaris</i>	10
Knowledge-Based Decision Support with Self-Learning Methods <i>Klaus Peter Scherer, Constantin Rieder, Markus Germann, Joachim Baumeister, and Stefan Plehn</i>	15
An Innovative Crowd Segmentation Approach based on Social Force Modelling <i>Yu Hao, Zhijie Xu, Ying Liu, Jing Wang, and Jiulun Fan</i>	18
Speeding up the Recommender Systems by Excluding the Low Rated Items <i>Yousef Kilani</i>	24
CLINIC: A Web Healthcare Management System for Enhancing Clinical Services <i>Ahmad Qawasmeh, Dema Awni, Raghad Mohammed, Rufaida Sabri, and Ghydaa Ahmad</i>	28

Time Series Forecasting using ARIMA Model

A Case Study of Mining Face Drilling Rig

Hussan Al-Chalabi, Yamur K. Al-Douri and Jan Lundberg

Division of Operation and Maintenance Engineering

Luleå University of Technology

Luleå, Sweden

E-mail: {hussan.hamodi, yamur.aldouri, jan.lundberg}@ltu.se

Abstract— This study implements an Autoregressive Integrated Moving Average (ARIMA) model to forecast total cost of a face drilling rig used in the Swedish mining industry. The ARIMA model shows different forecasting abilities using different values of ARIMA parameters (p , d , q). However, better estimation for the ARIMA parameters is required for accurate forecasting. Artificial intelligence, such as multi objective genetic algorithm based on the ARIMA model, could provide other possibilities for estimating the parameters. Time series forecasting is widely used for production control, production planning, optimizing industrial processes and economic planning. Therefore, the forecasted total cost data of the face drilling rig can be used for life cycle cost analysis to estimate the optimal replacement time of this rig.

Keywords- ARIMA model; Data forecasting; Mining face drilling rig.

I. INTRODUCTION

Time series forecasting predicts future data points based on observed data over a period known as the lead-time. The purpose of forecasting data points is to provide a basis for production control and production planning and to optimize industrial processes and economic planning. The major objective is to obtain the best forecast, i.e., to ensure that the mean square of the deviation between the actual and the forecasted values is as small as possible for each lead-time [1]. Over the past few decades, much effort has been devoted to the development and improvement of time series forecasting models [2].

Traditional models for time series forecasting, such as the Box–Jenkins or the Autoregressive Integrated Moving Average (ARIMA) model, assume time series data are generated by linear processes. However, these models may be inappropriate if the underlying mechanism is nonlinear. In fact, real-world systems are often nonlinear [3]. The ARIMA model is a stochastic process [1] defined by three parameters, p , d , and q , where p stands for the Auto-Regressive $AR(p)$ process, d is the integration (needed for the transformation into a stationary stochastic process), and q is the Moving Average $MA(q)$ process [4].

In a stationary stochastic model, the data have the same variance and autocorrelation [5]. The weakness of this model is the difficulty of estimating the parameters. To address this problem and ensure accurate forecasting, we need a process for automated model selection [6].

Zhang [7] suggests a hybrid method that combines ARIMA and Artificial Neural Network

(ANN) models. The combination improves the forecasting accuracy. The empirical results with three real data sets clearly show the hybrid model is able to outperform each component model. There are some similarities between ARIMA and ANN models. Both include a rich class of different models with different model orders. Both require a relatively large sample to build a successful model. However, ARIMA can provide results based on the problem and data contents.

Hatzakis and Wallace [8] propose a method that combines the ARIMA forecasting technique and a Multi Objective Genetic Algorithm (MOGA) based on Pareto optimality. Their method is based on historical optimums and is used to optimize $AR(p)$ and $MA(q)$ to find a non-dominated Pareto front solution with an infinite number of points. They found that their method improved the prediction accuracy. However, they assumed the data were accurate and used the Pareto front solution to make a forecast.

This study implements an ARIMA model to forecast the Total Cost (TC) data for a face drilling rig used in an underground mine in Sweden. Findings from our case study suggest that the ARIMA model is appropriate, but the parameters need to be better estimated for accurate forecasting.

The remainder of the paper is structured as follows: In Section II, we define the research paper methodology. In Section III, we present the results and discussion. We conclude the paper in Section IV.

II. METHODOLOGY

A. Data collection

The TC data are for a face drilling rig used in an underground mine in Sweden. The data were collected over a period of three years (2009 to 2012) by a MAXIMO Computerized Maintenance Management System (CMMS). In the CMMS, the TC data are recorded based on the work orders for the maintenance of the face drilling rig. Every work order contains corrective maintenance cost data, a component problem description, and a description of the actions performed (i.e., corrective maintenance or preventive maintenance). The repair time and the labour, material and tool cost of each work order are also included.

In this study, missing and outlier data are filtered from the selected TC data. Note that all the cost data used in this

study are real costs with no adjustment for inflation. Note also that because of mining company regulations, the TC data are encoded and expressed as a Currency Unit (cu).

B. ARIMA model

The main part of the ARIMA model combines *AR* and *MA* polynomials into a complex polynomial, as seen in (1) below [9]. The ARIMA (*p, d, q*) model is applied to all the data points of the TC data.

$$y_t = \mu + \sum_{i=1}^p (\sigma y_{t-i}) + \sum_{i=1}^q (\theta \varepsilon_{t-i}) + \varepsilon_t \tag{1}$$

where the notation is as follows:

- μ : the mean value of the time series data;
- p : the number of autoregressive lags;
- σ : autoregressive coefficients (*AR*);
- q : the number of lags of the moving average process;
- θ : moving average coefficients (*MA*);
- ε : the white noise of the time series data;
- d : the number of differences calculated from (2)

$$\Delta y_t = y_t - y_{t-1} \tag{2}$$

The value of the ARIMA parameters (*p, d, q*) for *AR* and *MA* can be obtained from the behaviour of the Autocorrelation Function (ACF) and the Partial Autocorrelation Function (PACF) [1]. These functions help to estimate the parameters that can be used to forecast data using the ARIMA model.

III. RESULTS AND DISCUSSION

The ARIMA model is implemented stochastically based on the default values of the parameters *p, d* and *q* for the different scenarios individually for TC (Z^{TC}). The values for each parameter (*p, d, q*) are: (0,0,0), (0,0,1), (0,1,1), (1,0,0), (1,0,1), (1,1,1), (2,1,1) and (2,0,3). All the TC data are included for each scenario, covering a period of 37 months. The forecasting is for 24 months. Some scenarios do not show a reasonable forecasting for this period. In this section, we present the TC forecasting using the ARIMA parameters (1,0,1), (0,0,1), (2,1,1) and (2,0,3) as the default input parameters.

Figure 1 shows the forecasting for ARIMA (1,0,1) for the log of TC over time (24 months). A polynomial trend curve is used to illustrate the relationship between the historical TC data and the forecasted data. The historical TC data (37 months) appear before the vertical line. The forecasted data (24 months) are presented after the vertical line. The forecasted data for ARIMA (1,0,1) seem to be in sync with the historical data before the vertical line and with the polynomial trend curve after the vertical line. This is obvious because the forecasted data show a polynomial trend curve. However, there are lower and higher extreme forecasted values outside the polynomial trend.

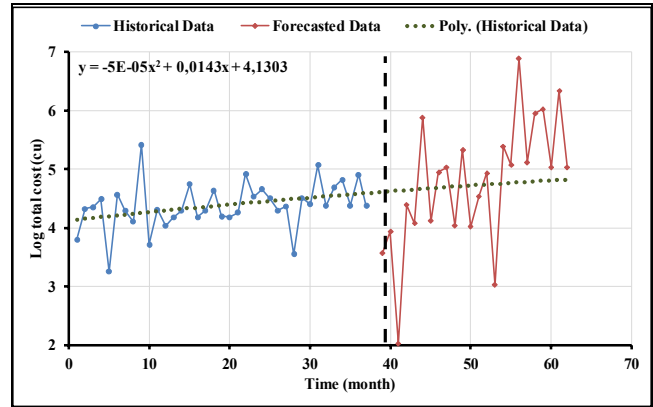


Figure 1. ARIMA (1, 0, 1)

The results of ARIMA (0, 0, 1) are shown in Figure 2. After the vertical line, the forecasted data for the 24-month period do not seem to be in sync with the historical data before the vertical line or with the polynomial trend curve after the vertical line.

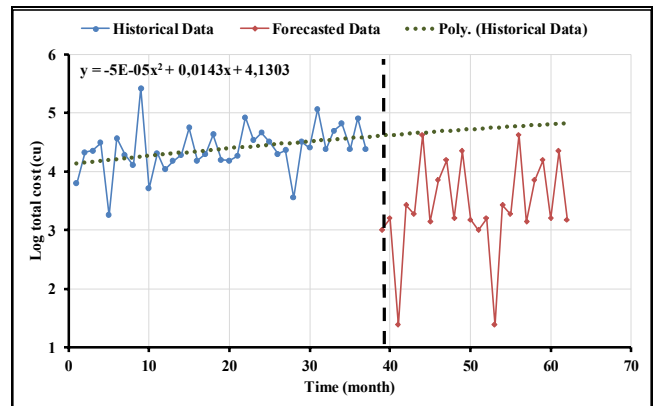


Figure 2. ARIMA (0, 0, 1)

Figure 3 shows the results for ARIMA (2,1,1) for the TC with the polynomial trend curve. The forecasted data for the 24-month period do not seem to be in sync with the historical data before the vertical line or with the polynomial trend curve after the vertical line. The forecasted data are much higher than the historical and polynomial trends.

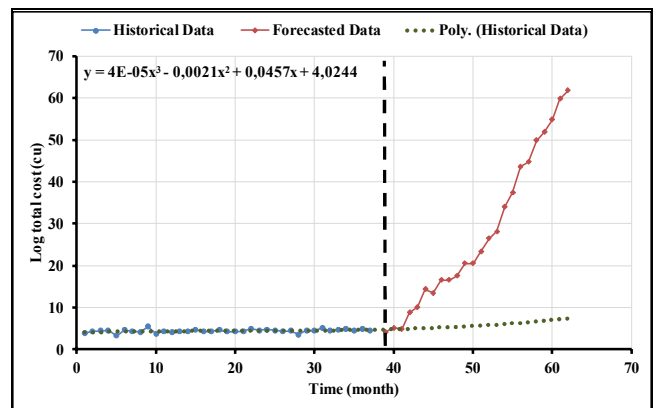


Figure 3. ARIMA (2, 1, 1)

The results of ARIMA (2,0,3) are shown in Figure 4. In the figure, the forecasted data for the 24-month period seem to be in sync with the historical data before the vertical line and with the polynomial trend curve after the vertical line. Accordingly, these parameters are suitable for forecasting the TC data for this mining drilling rig.

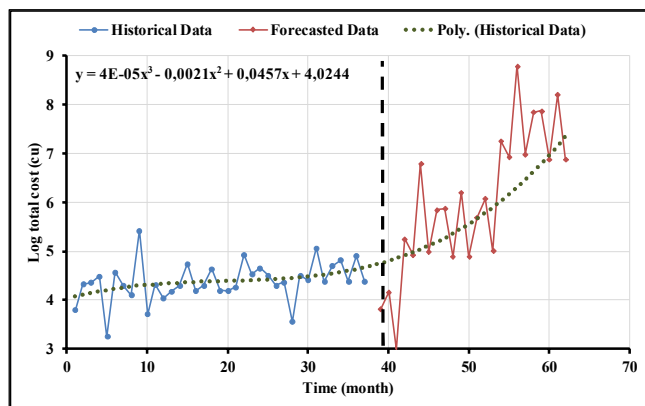


Figure 4. ARIMA (2,0,3)

Overall, the forecasting using ARIMA (2,0,3) has better results than forecasting using the other ARIMA input parameters. We also find that the values of (p, d, q) affect the ARIMA forecasting, and the ARIMA (p, d, q) values are sensitive to the data type.

IV. CONCLUSION AND FUTURE WORK

The forecasting for our case study using the ARIMA model shows different forecasting abilities using different values of ARIMA parameters (p, d, q) . The ARIMA parameters (p, d, q) are used in four different scenarios, one of which shows suitable forecasting. We find that the parameter values have a strong effect on the forecasting method. Therefore, these parameters need better estimation from the data for accurate forecasting. AI such as MOGA based on the ARIMA model could provide other possibilities for estimating the parameters (p, d, q) and improve data forecasting. The outcome of the MOGA based on the ARIMA model can be used to forecast data with a high level of accuracy, and the forecasted data can be used for life cycle cost analysis. For example, they can be used to estimate the optimal replacement time of the face drilling rig used in our case study.

ACKNOWLEDGMENT

The people at Boliden AB and Epiroc Rock Drills AB who helped in this research are gratefully acknowledged. The maintenance personnel and CMMS employees at Boliden AB who helped us in this research are also thanked for their support. In addition, we would like to extend our gratitude to Dr Ali Ismail Awad, Luleå University of Technology, Luleå, Sweden, for allowing us to use the computing facilities of the Information Security Laboratory to conduct the experiments in this study.

REFERENCES

- [1] G.E. Box, G.M. Jenkins, G.C. Reinsel and G.M. Ljung, Time series analysis: forecasting and control, 4th ed, John Wiley & Sons, 2016.
- [2] Y. Chen, B. Yang, J. Dong and A. Abraham, "Time-series forecasting using flexible neural tree model," *Inf.Sci.*, vol. 174, October 2004, pp. 219-235.
- [3] J.V. Hansen, J.B. McDonald, and R.D. Nelson, "Time Series Prediction With Genetic-Algorithm Designed Neural Networks: An Empirical Comparison With Modern Statistical Models", *Computational Intelligence*, vol. 15, 1999, pp. 171-184.
- [4] N.R. Herbst, N. Huber, S. Kounev and E. Amrehn, "Self adaptive workload classification and forecasting for proactive resource provisioning," *Concurrency and computation: practice and experience*, vol. 26, March 2014, pp. 2053-2078.
- [5] D. Kwiatkowski, P.C. Phillips, P. Schmidt and Y. Shin, "Testing the null hypothesis of stationarity against the alternative of a unit root: How sure are we that economic time series have a unit root," *J. of Econometrics*, vol. 54, 1992, pp. 159-178.
- [6] R.J. Hyndman and Y. Khandakar, *Automatic time series for forecasting: the forecast package for R*, Monash University, Department of Econometrics and Business Statistics, 2007.
- [7] G.P. Zhang, "Time series forecasting using a hybrid ARIMA and neural network model," *Neurocomputing*, vol. 50, 2003, pp. 159-175.
- [8] I. Hatzakis and D. Wallace, "Dynamic multi-objective optimization with evolutionary algorithms: a forward-looking approach," in *Proceedings of the 8th annual conference on Genetic and evolutionary computation*, July 2006, pp. 1201-1208.
- [9] T. Vantuch and I. Zelinka, "Evolutionary based ARIMA models for stock price forecasting," in *ISCS 2014: Interdisciplinary Symposium on Complex Systems*, vol. 14, 2015, pp. 239-247.

Time Series Forecasting using Genetic Algorithm

A Case Study of Maintenance Cost Data For Tunnel Fans

Yamur K. Al-Douri, Hussan Al-Chalabi, Jan Lundberg

Division of Operation and Maintenance Engineering

Luleå University of Technology

Luleå, Sweden

emails: {yamur.aldouri, hussan.hamodi, jan.lundberg}@ltu.se

Abstract— Time series forecasting is widely used as a basis for economic planning, production planning, production control and optimizing industrial processes. The aim of this study has been to develop a novel two-level Genetic Algorithm (GA) to optimize time series forecasting in order to forecast cost data for fans used in road tunnels by the Swedish Transport Administration (Trafikverket). The first level of the GA is responsible for the process of forecasting time series cost data, while the second level evaluates the forecasting. The first level implements GA based on the Autoregressive Integrated Moving Average (ARIMA) model. The second level utilizes a GA based on forecasting error rate to identify proper forecasting. The results show that GA based on the ARIMA model produces good forecasting results for the labor cost data objects. It was found that a multi-objective GA based on the ARIMA model showed an improved performance. The forecasted data can be used for Life Cycle Cost (LCC) analysis.

Keywords— ARIMA model; Time series forecasting; Genetic Algorithm (GA); Life Cycle Cost (LCC); Maintenance cost data.

I. INTRODUCTION

Time series forecasting predicts future data points based on observed data over a period known as the lead-time. The purpose of forecasting data points is to provide a basis for economic planning, production planning, production control and optimizing industrial processes. The major objective is to obtain the best forecast function, i.e., to ensure that the mean square of the deviation between the actual and the forecasted values is as small as possible for each lead-time [1]. Much effort has been devoted over the past few decades to the development and improvement of time series forecasting models [2].

The Genetic Algorithm (GA) is often compatible with nonlinear systems and uses a particular optimization from the principle of natural selection of the optimal solution on a wide range of forecasting populations [3]. The proposed multi-objective GA optimizes a particular function based on the ARIMA model. The ARIMA model is a stochastic process modelling framework [4] that is defined by three parameters (p, d, q). The parameter p stands for the order of the autoregressive AR(p) process, d for the order of integration (needed for the transformation into a stationary

stochastic process), and q for the order of the moving average MA(q) process [4]. A stationary stochastic process means a process where the data properties have the same variance and autocorrelation [5].

The weakness of the ARIMA model is the difficulty of estimating the parameters. To address this problem, a process for automated model selection needs to be implemented in the automated optimization to achieve an accurate forecasting [6]. The GA is a well-established method which helps in solving complex and nonlinear problems that often lead to cases where the search space shows a curvy landscape with numerous local minima. The GA is designed to find the best forecasting solution through automated optimization of the ARIMA model and to select the best parameters (p, d, q) to compute point forecasts based on time series data. The parameters of the ARIMA model are influenced by the selecting process of the GA. In addition, the GA can evaluate the forecasting accuracy using multiple fitness functions based on statistics models.

Vantuch & Zelinka [7] modified the ARIMA model based on the Genetic Algorithm and particle swarm optimization (PSO) to estimate and predict data of time. They found that the Genetic Algorithm could find a suitable ARIMA model and pointed to improvements through individual binary randomization for every parameter input of the ARIMA model. Their model shows the best set of coefficients obtained with PSO compared with the best set obtained with a classical ARIMA prediction. However, these authors present the ARIMA parameters in a binary setting with limited possibilities and they consider the forecasting based on an ARIMA evaluation only.

Hatzakis & Wallace [3] proposed a method that combines the ARIMA forecasting technique and a multi-objective GA based on the Pareto optimal to predict the next optimum. Their method is based on historical optimums and is used to optimize AR(p) and MA(q) to find a non-dominated Pareto front solution with an infinite number of points. They found that their method improved the prediction accuracy. However, these authors assumed that the data were accurate and used the Pareto front solution to select a proper forecasting. In addition, they did

not use any forecasting error rate to evaluate the forecasting results.

The aim of this study has been to develop a novel two-level multi-objective GA to optimize time series forecasting in order to forecast cost data for fans used in road tunnels. The first level of the GA is responsible for the process of forecasting time series cost data, while the second level evaluates the forecasting. The first level implements GA based on the ARIMA model. This level gives possibilities of finding the optimal forecasting solution. The second level utilizes GA based on forecasting error rate to identify a proper forecasting. We argue that a GA decreases the complexity, increases the flexibility, and is very effective when selecting an approximate solution interval for forecasting.

II. METHODOLOGY

A. Data collection

The cost data concerns tunnel fans installed in Stockholm in Sweden. The data had been collected over ten years from 2005 to 2015 by Swedish Transport Administration (Trafikverket) and were stored in the MAXIMO computerized maintenance management system (CMMS). In this CMMS, the cost data are recorded based on the work orders for the maintenance of the tunnel fans. Every work order contains corrective maintenance data, a component description, the reporting date, a problem description, and a description of the actions performed. Also included are the repair time needed and the labor, material and tool cost of each work order.

In this study, we consider the one cost objects of labor based on the work order input into the CMMS for the ten-year period mentioned above. The selected data were clustered, filtered and inputed for the present study using a Multi-objective GA (MOGA) based on a fuzzy c-means algorithm [14]. It is important to mention that all the cost data used in this study concern real costs without any adjustment for inflation. Due to company regulations, all the cost data have been encoded and are expressed as currency units (cu).

B. Two-level system of Genetic Algorithms

In this study, a novel two-level GA has been developed, as shown in Figure 1. The levels of the GA are as follows: (1) a GA based on the ARIMA model for forecasting the cost data, and (2) GA based on multiple functions for measuring the forecasting accuracy for validation of the forecasted data. Level 1 of the GA is applied to the cost data objects (labor) to forecast data for the next level and for each of 15 different generations. The second level validates the forecasted data for the cost object. Using two levels allows us to reduce the computational cost [8], while reaching an effective and reasonable solution [9].

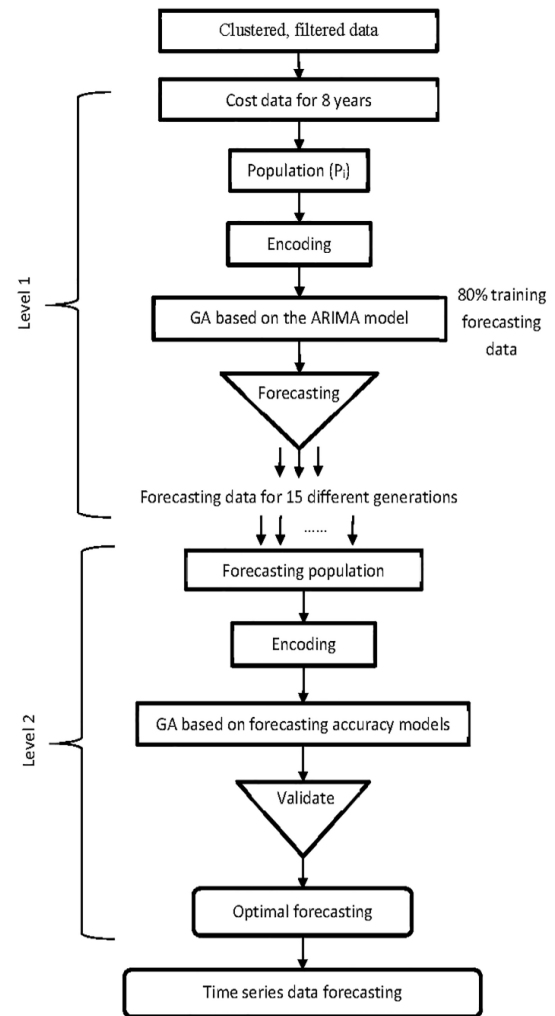


Figure 1. Two-level of Genetic Algorithm (GA)

1) GA based on the ARIMA model

The proposed GA method uses a particular optimization based on the principle of natural selection of the optimal solution and applies this optimization on a wide range of forecasting **populations**. The GA creates populations of **chromosomes** as possible answers to estimate the optimum forecasting [3]. This algorithm is robust, generic and easily adaptable because it can be broken down into the following steps: initialization, evaluation, selection, crossover, mutation, update and completion. The evaluation (**fitness function**) step creates the basis for a new population of chromosomes. The new population is formed using specific Genetic operators, such as **crossover** and **mutation** [10], [11]. The fitness function is derived from the ARIMA forecasting model. A GA with automated optimization avoids the weakness of the ARIMA model by estimating the parameters for forecasting [6].

The GA is a global optimization technique that can be used to achieve an accurate forecasting based on the ARIMA model. The GA is known to help in solving

complex nonlinear problems that often lead to cases where the search space shows a curvy landscape with numerous local minima. Moreover, the GA is designed to find the optimal forecasting solution through automated optimization of the ARIMA model. In addition, the GA can evaluate the forecasting accuracy using multiple fitness functions based on statistical models.

The first level utilizes a GA which is based on the ARIMA model and is implemented four different times using a cross-validation randomization technique. The technique aims to select the best time series data for forecasting. The process is the following: a random number of cost data are selected based on encoding in each of the four implementations; the modified random cost data are generated 15 times. The modifications are used to find the optimal cost data for forecasting. The following steps are implemented when applying the multi-objective GA in level 1.

Step 1: Initial population

A longitudinal study of each cost object ($Z^{labour}, Z^{material}$) is used to forecast data using the multi-objective GA for the two objects in parallel.

Step 2: First GA generation and selection

The first generation is performed by selecting each cost object and checking whether the data are stationary (i.e., trend-stationary) or non-stationary using a Dickey-Fuller test [12]. To apply the ARIMA model, the data should be stationary, i.e. the null hypothesis of stationarity should not be rejected. When applying the Dickey-Fuller Test (DFT) in equation (1), the hypothesis $p = 1$ means that the data are non-stationary and $p < 1$ that the data are stationary [12].

$$DFT(x_t) = \alpha + px_{t-k} + \epsilon_t \quad (1)$$

α : constant estimated value of the time series data;

p : the hypothesis is either $p = 1$ or $p < 1$;

t : time $\{1, \dots, k\}$;

ϵ : the white noise of the time series data.

Step 3: Encoding

Random values, either ones or zeros, are generated for each cost data object. Encoding is the process of transforming from the phenotype to the genotype space before proceeding with GA operators and finding the local optima.

Step 4: Fitness function

The fitness function is based on the ARIMA model for the forecasting of time series cost data objects individually, as seen in the equation below. The fitness function consists of an autoregression (AR) part and a moving average (MA) part [1]. The ARIMA model uses AR and MA polynomials to estimate (p) and (q) [7].

The fitness function is formulated as the equation (2) follows:

$$fitness(p, d, q) = \mu + \sum_{i=1}^p (\sigma y_{t-1}) + \sum_{i=1}^q (\theta \epsilon_{t-1}) + \epsilon_t \quad (2)$$

where the following notation is used:

μ : the mean value of the time series data;

p : the number of autoregressive lags;

d : the number of differences calculated with the equation $\Delta y_t = y_t - y_{t-1}$;

q : the number of lags of the moving average process;

σ : autoregressive coefficients (AR);

θ : moving average coefficients (MA);

ϵ : the white noise of the time series data.

The parameters (p,q) are estimated using an autocorrelation function (ACF) and a partial autocorrelation function (PACF) [1]. The estimated values produced by the previous equation will be used to create a forecast for 20 months (m) using the equation (3). These forecasted values will be evaluated using the second level of GA to find the optimal forecasting with high accuracy.

$$fitness(t + m) = \mu + \sum_{i=1}^p (\sigma y_{t-1}) + \sum_{i=1}^q (\theta \epsilon_{t-1}) + \epsilon_t \quad (3)$$

where fitness(t+m) is the time series forecasting at time (t+m) and

m : months $\{1, 2, 3, \dots, m\}$.

Step 5: Crossover and mutation

In this study, a one-point crossover with a fixed crossover probability is used. This probability decreases the bias of the results over different generations caused by the huge data values. For chromosomes of length l, a crossover point is generated in the range [1, 1/2 l] and [1/2 l, l]. The values of objects are connected and should be exchanged to produce two new offspring. We select two points to create more value ranges and find the best fit.

Randomly, ten percent of the selected chromosomes undergo mutation with the arrival of new chromosomes. For the cost object values, we swap two opposite data values. The purpose of this small mutation percentage is to keep the forecasting changes steady over different generations.

Step 6: New generation

The new generation step repeats steps 3 to 5 continuously for 15 generations. Fifteen generations are enough for these data because the curves of the fitness functions are repeated after fifteen generations. The selected fifteen generations are used individually for the second level to validate the forecasting accuracy for each object and population. This step yields fully correlated data for the next step.

2) GA for measuring the forecasting accuracy

In this level, the GA is applied longitudinally to the data. The GA operates with a population of chromosomes that contains labor cost and material cost objects. The GA operates on the selected population over different generations to find the appropriate forecasting accuracy. During the GA generations, the chromosomes in the population are rated concerning their adaptation, and their

mechanism of selection for the new population is evaluated. Their adaptability (fitness function) is the basis for a new population of chromosomes. The new population is formed using specific Genetic operators such as crossover and mutation. The GA is used to evaluate the forecasting accuracy for each generation of the first level.

Level 2 utilizes a GA which is based on different forecasting error rates and is implemented for each generation from the first level and for four different populations using a cross-validation randomization technique. This technique aims to select the best evaluation of the time series data forecasting and the process is as follows. A random number of cost data are selected based on the encoding in each generation of the four implementations, and the modified random cost data are generated five times. The modifications are then used to find the optimal cost data forecasting. In this study, due to the size of the training data, five generations are sufficient to obtain valid results. The following steps are implemented when applying the GA in level 2.

Step 1: Initial population

A longitudinal study of each cost object ($Z^{labour}, Z^{material}$) is used to forecast data using the multi-objective GA for the two objects in parallel.

Step 2: First GA generation, encoding and selection

The first generation is performed by selecting each cost object and encoding through generating random values, either ones or zeros, for each cost data object. The selection for each cost data object is based on encodings with the value of 1. This selection is used to evaluate the forecasted data using the multi-objective fitness function.

Step 3: Fitness function

The multi-objective fitness function is based on multiple functions for measuring the forecasting accuracy. The mean absolute percentage error (MAPE) is used to evaluate the selected forecasting data from the previous step [13]. The fitness functions are formulated as equation (4):

$$fitness(MAPE) = mean(|p_i|) \quad (4)$$

where

$$p_i = \frac{100e_i}{Y_i} \text{ and } e_i = Y_i - F_i$$

t : time $\{1, \dots, k\}$;

Y_t : the actual data over time;

F_t : the forecasted data over time.

Step 4: Crossover and mutation

In this study, we use a one-point crossover with a fixed crossover probability. This probability decreases the bias of the results over different generations due to the huge data values. For chromosomes of length l , a crossover point is generated in the range $[1, 1/2 l]$ and $[1/2 l, l]$. The values of objects are connected and should be exchanged to produce two new offspring. We select two points to create more value ranges and find the best fit.

Randomly ten percent of the selected chromosomes undergo mutation with the arrival of new chromosomes. For the cost object values, we swap two opposite data values. The purpose of this small mutation percentage is to keep the forecasting changes steady over different generations.

Step 5: New generation

The new generation step repeats steps 2 to 4 continuously for five generations. Five generations are enough for these data, because the fitness function is repeated after the fifth generation. The selected generation is used for the second level to validate the forecasting accuracy for each object. This step yields fully correlated data that can be used for forecasts covering several months.

III. RESULTS OF THE TWO-LEVEL GAS

A. Results of Level 1: GA based on the ARIMA model

In this part of the study, we tested GA based on the ARIMA model to generate forecasting data for the labor cost object. The forecasted data for each population obtained with 15 different generations were then evaluated using the second level. The second level evaluation helped in deciding the best generation of the forecasted data. In this section, we present only the best forecasted curves with the historical data because of the huge number of possibilities considered in this study.

Figure 2 shows the forecasted labor data curve for 20 months from 2013 to 2015, for the second population and, specifically, for generation 13. In addition, it shows the historical data with the polynomial trend to illustrate the relationship between the independent variables over a timeline with monthly intervals. The selected labor data show a better forecasting than that obtained with the ARIMA model in that the forecasted data are close to the actual data and the polynomial trend. The ARIMA parameters for the selected labor cost data covering 47 months were $p=0.22, d=1$ and $q=0.23$.

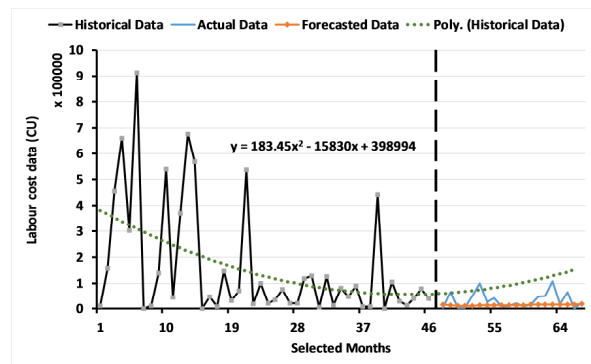


Figure 2. Labor cost data forecasting using the GA based on the ARIMA model

The forecasted data for the labor cost object were evaluated using the second level, applying a GA based on the statistical forecasting error rate. The model for the forecasting accuracy evaluated the forecasted data for 20 months from 2013 to 2015 based on the actual values of this period. Implementing level 2, the accurate forecasted

data were found, i.e. the proper selection of data for each object to be used for forecasting.

Figure 3 show an example of bias in forecasting at the second population and seventh generation. The forecasted data for the 20-month period do not seem to be in sync with the historical data before the vertical line or with the polynomial trend curve after the vertical line. The forecasted data are higher than the historical and polynomial trends.

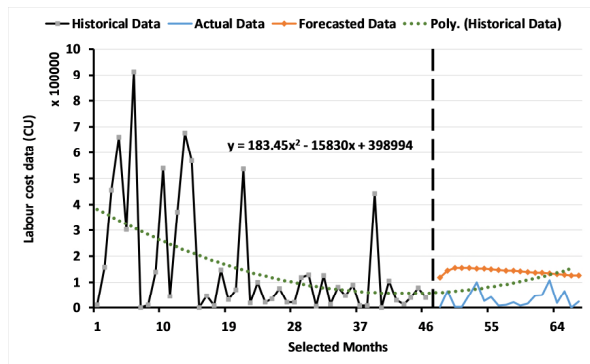


Figure 3. Labor cost data forecasting using the GA based on the ARIMA model

B. Results of level 2: GA for measuring the forecasting accuracy

The outcome from the first level, specifically for each generation for each population, indicates the forecasting accuracy for each cost object. For each generation, the GA based on multiple fitness functions was used to find the best fitness value through five different generations. The fitness functions (forecasting error rate models) provide an accurate data forecasting through comparing the behaviour of the different models and revealing which forecasting model is appropriate.

Selecting a proper population for the labor cost data is quite difficult due to the variety of fitness values. In this study, we considered the population that was selected by fitness value that have a low forecasting error rate. The twelve generation for the forth population was selected as having the lowest forecasting error rate with a suitable selection of input data. The labor cost data were selected using fitness (MAPE), with value of 0.4 as seen in Figure 4.

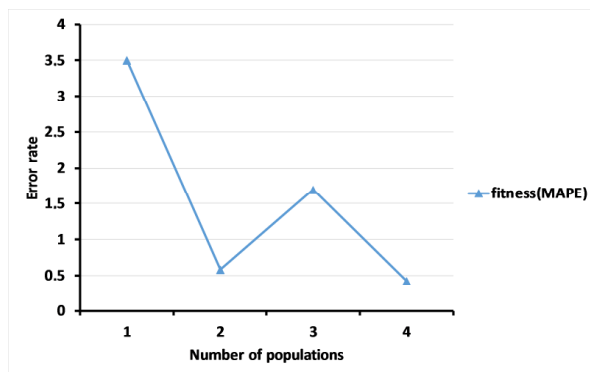


Figure 4. Fitness(MAPE) for four populations

IV. CONCLUSIONS

The GA based on the ARIMA model provides other possibilities for calculating the parameters (p,d,q) and improves the data forecasting. The outcome of the multi-objective GA based on the ARIMA model can be used to forecast data with a high level of accuracy, and the forecasted data can be used for LCC analysis.

ACKNOWLEDGMENT

The authors would like to thank Dr. Ali Ismail Awad, Luleå University of Technology, Luleå, Sweden, for his support concerning the research methodology and for allowing us to use the computing facilities of the Information Security Laboratory to conduct the experiments in this study. In addition, we would like to extend our gratitude to Prof. Peter Soderholm at the Swedish Transport Administration (Trafikverket) for supplying the data for this study.

REFERENCES

- [1] G. E. Box, G.M. Jenkins, G.C. Reinsel and G.M. Ljung, Time series analysis: forecasting and control, John Wiley & Sons, 2015.
- [2] Y. Chen, B. Yang, J. Dong and A. Abraham, "Time-series forecasting using flexible neural tree model," Inf.Sci., vol. 174, no. 3, pp. 219-235, 2005.
- [3] I. Hatzakis and D. Wallace, "Dynamic multi-objective optimization with evolutionary algorithms: a forward-looking approach," in Proceedings of the 8th annual conference on Genetic and evolutionary computation, 2006, pp. 1201-1208.
- [4] N. R. Herbst, N. Huber, S. Kounev and E. Amrehn, "Self-adaptive workload classification and forecasting for proactive resource provisioning," Concurrency and computation: practice and experience, vol. 26, no. 12, pp. 2053-2078, 2014.
- [5] D. Kwiatkowski, P.C. Phillips, P. Schmidt and Y. Shin, "Testing the null hypothesis of stationarity against the alternative of a unit root: How sure are we that economic time series have a unit root?" J.Econ., vol. 54, no. 1-3, pp. 159-178, 1992.
- [6] R. J. Hyndman and Y. Khandakar, Automatic time series for forecasting: the forecast package for R, Monash University, Department of Econometrics and Business Statistics, 2007.
- [7] T. Vantuch and I. Zelinka, "Evolutionary based ARIMA models for stock price forecasting," in ISCS 2014: Interdisciplinary Symposium on Complex Systems, 2015, pp. 239-247.
- [8] S. Thomassey and M. Happiette, "A neural clustering and classification system for sales forecasting of new apparel items," Applied Soft Computing, vol. 7, no. 4, pp. 1177-1187, 2007.
- [9] C. Ding, Y. Cheng and M. He, "Two-level Genetic Algorithm for clustered traveling salesman problem with application in large-scale TSPs," Tsinghua Science & Technology, vol. 12, no. 4, pp. 459-465, 2007.
- [10] O. Cordon, F. Herrera, F. Gomide, F. Hoffmann and L. Magdalena, "Ten years of Genetic fuzzy systems: current framework and new trends," in IFSA World Congress and 20th NAFIPS International Conference, 2001. Joint 9th, 2001, pp. 1241-1246.

- [11] C. Shi, Y. Cai, D. Fu, Y. Dong and B. Wu, "A link clustering based overlapping community detection algorithm," *Data Knowl.Eng.*, vol. 87, pp. 394-404, 2013.
- [12] S. J. Leybourne, T.C. Mills and P. Newbold, "Spurious rejections by Dickey–Fuller tests in the presence of a break under the null," *J.Econ.*, vol. 87, no. 1, pp. 191-203, 1998.
- [13] R. J. Hyndman and A.B. Koehler, "Another look at measures of forecast accuracy," *Int.J.Forecast.*, vol. 22, no. 4, pp. 679-688, 2006.
- [14] Yamur K. Aldouri, Hassan Al-Chalabi, and Zhang Liangwei. "Data clustering and imputing using a two-level multi-objective genetic algorithm (GA): A case study of maintenance cost data for tunnel fans." *Cogent Engineering* 5.1: 1-16, 2018.

Hierarchical Multi-Scale Computational Methodologies for the Study of Complex Molecular Systems

Georgios Kritikos^{1*}, Anthony Chazirakis¹, Petra Bačová¹, Anastassia N. Rissanou¹, Evangelia Kalligiannaki¹, and Vagelis Harmandaris^{1,2}

¹Institute of Applied and Computational Mathematics (IACM),
Foundation for Research and Technology Hellas (FORTH),
Heraklion, Crete, Greece.

²Department of Mathematics and Applied Mathematics,
University of Crete,
Heraklion, Crete, Greece.

e-mails: kritikgio@iacm.forth.gr, achazirakis@iacm.forth.gr, pbacova@iacm.forth.gr, rissanou@iesl.forth.gr, evangelia.kalligiannaki@iacm.forth.gr, harman@uoc.gr

Abstract—Here, we give a short overview of hierarchical multi-scale simulation methodologies for predicting structure-property relations of macromolecular systems. In the first stage, detailed microscopic (atomistic) Molecular Dynamics (MD) simulations are performed. Various properties related to thermodynamics, structure and dynamics of polymeric systems are being examined at the atomistic level. In the second stage, our work involves an extension to a mesoscopic, Coarse Grained (CG) description of the simulated systems. Finally, CG simulations of larger systems and for longer times are performed. The proposed approach allows us to extend the simulated spatio-temporal scales of macromolecular systems.

Keywords—Hierarchical modeling; Multi-scale; Molecular dynamics simulation; Coarse-graining.

I. INTRODUCTION

Design and innovation in materials science requires nowadays the use of computer simulations. As the computational power continuously improves, it is possible to study, using molecular simulations, multiphase and nanocomposites systems with various applications in energy storage, biomaterials, elastomers, electronics, etc. [1]–[3]. By employing Molecular Dynamics (MD) simulations and having an accurate force field that is parameterized on quantum calculations, someone can reproduce the dynamics at bulk or interphases and extract information about interfacial properties. Nevertheless, the representation at the atomistic level does not always permit us to model realistic systems, due to the enormous range of length and time scales associated with complex macromolecular-based materials [1][4]. Therefore, the investigation of the structural and dynamical properties in complex molecular systems requires dimensionality reduction techniques. Such a technique is the Coarse Graining (CG), in which a group of atoms is represented as a CG super-atom. The CG level of representation allows the description of the involved structure and dynamics, and the temperature dependence of

various properties, such as the density, the heat capacity, the viscosity, the modulus, etc., with fewer parameters [5][6]. Thus, hierarchical multi-scale computational methods can provide low cost tools for the industrial design of materials, but also for answering fundamental questions in soft matter science.

Coarse graining can be realized as a procedure of mapping the microscopic (atomistic) space, determined by N particles, $q = (q_1, \dots, q_N) \in R^{3N}$, to a CG, mesoscopic space of fewer M particles [7], i.e., $q \mapsto Q$ where $Q \in R^{3M}$ and $M < N$. The probability of a certain macromolecular configuration in the microscopic space should be the same with the probability of the same configuration in the CG representation, in the mesoscopic space, thus the corresponding CG potential of the super-atom should incorporate the free energy of the building atoms.

The n -body Potential of Mean Force (PMF) can be defined as [7]:

$$\bar{U}^{(n),PMF}(Q^{(n)}) = -k_B T \ln g^{(n)}(Q^{(n)}), \quad n < M, \quad (1)$$

through the n -body distribution function, $g^{(n)}(Q^{(n)})$, where $Q^{(n)}$ are the coordinates of the n particles [7]. In practice, usually the pair ($n=2$) distribution function is used. Then, the CG force field is based on the mean force:

$$\bar{F}_i^{PMF}(Q) = -\nabla_{Q_i} \bar{U}^{PMF}(Q), \quad i = 1, \dots, M. \quad (2)$$

The first step towards the mesoscopic representation is the definition of the CG sites/super-atoms. Usually, in a low degree of CG, 5-10 atoms or 1-2 monomers constitute a super-atom [5][7]. The advantage of such a mapping scheme is that it retains the ability to predict properties at the atomistic level, while at the same time it is possible for the equilibrated CG system to re-insert atomistic detail following a back-mapping procedure [5]. An example of PolyStyrene (PS) mapping onto CG representation has been presented in [5][8] and is depicted in Figure 1.

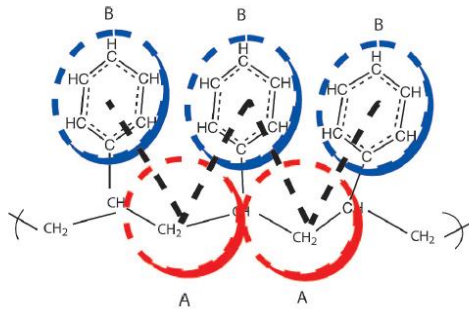


Figure 1. Representation of PS in atomistic and CG scale [5].

In the next step, we are interested in the development of a force field that governs the CG simulation. There exist several methods that allow the derivation of the CG potentials, based on (mainly structural) data derived from detailed atomistic simulations. All of them are characterized by an observable Φ and a minimization over a set of parameters Θ (cost functions) [7]. In structural or correlation methods the observable is the pair radial distribution function, $g(r)$. In the Force Matching (FM) or Multi Scale (MS) CG methods we focus on the description of the forces acting on a CG bead in order to reproduce the atomistic dynamics. Also, in the Relative Entropy (RE) approach the observable is related to the microscopic probability distribution [7].

For the intramolecular potentials that determine the internal structure of the macromolecule, in most cases we assume that they are described by the product of the probability distribution of each of the potentials [9]:

$$P(l, \theta, \varphi) = P(l)P(\theta)P(\varphi), \quad (3)$$

where $P(l)$, $P(\theta)$ and $P(\varphi)$ refer to the distribution of the CG bond lengths, the angle between three consequent CG super-atoms and the dihedral angle formed by four consequent CG super-atoms respectively. The probability is defined based on the Boltzmann factor:

$$P_i = \exp\left(-\frac{U_i}{k_B T}\right), \quad i = l, \theta, \varphi. \quad (4)$$

Concerning the effective PMF (\bar{U}_{eff}) that defines the non-bonded interaction in the CG level, several numerical methods have been presented in the literature [1][2][4][7]. The structure-based methods are the Direct or Iterative Boltzmann Inversion (DBI or IBI respectively) and the Inverse Monte Carlo (IMC) method [4]. The force matching techniques solve a typical least squares problem [10], while the relative entropy methods use stochastic optimization and Newton-Raphson approaches. In case of the interaction between a super-atom and a surface, the effective potential can be calculated at a fixed distance *via* the constraint force required to keep the bead at this specific distance [8]. The latter can be determined based on oligomeric chains and then used for the description of longer polymeric chains, i.e., higher molecular weights.

In order to produce CG dynamics consistent with the atomistic simulation, one typical way is the use of the

stochastic Langevin method [11] based on the equation of motion [9]:

$$m \frac{d^2 \vec{r}_a}{dt^2} = -\nabla \bar{U}_{eff}^a - m\Gamma \frac{d\vec{r}_a}{dt} + \vec{W}_a(t), \quad (5)$$

where m is the mass of the particle a , Γ is the background friction and \vec{W} is the statistical force of the heat bath. The use of a friction coefficient can allow us to correct the acceleration in the CG dynamics that is usually present due to the reduction in the degrees of freedoms compared to the atomistic representation [1].

The main goal of this work is to present the CG methodology focusing on polymer-based nanocomposites, i.e. a polymer matrix with nanoparticles or graphene as an additive phase. We intend to investigate the structural and dynamical properties at the polymer/nanofiller interface. The long relaxations times involved in such systems, even at temperatures well above the glass transition temperature (T_g), highlight the need for a mesoscopic approach. For this reason, the two stages of the hierarchical multi-scale methodology are elucidated. The first part includes atomistic simulations and the second part refers to the derivation of the needed CG force field for simulations at the mesoscopic level. As an example, a polyethylene (PE)/graphene nanocomposite is studied.

In the Section 2a, we present the parameters that describe the simulation at the atomistic level of PE in confined conditions formed by the presence of a modified (carboxylated) graphene sheet. In Section 2b, we give details of the CG procedure concerning the derivation of the force field for the simulation of the PE chain. Moreover, in Section 3, we present some preliminary results. The CG methodology is analyzed for the derivation of the non-bonded interactions, in the case of bulk PE. We close with Section 4, where the conclusions of our study and future plans are mentioned.

II. METHODOLOGY

A. Atomistic Simulation Details

The parameters of the force-field for PE were taken from the TraPPE (Transferable Potentials for Phase Equilibria) all-atom model [12] and in the case of the functionalized graphene we used the combination of all-atom OPLS (Optimized Potentials for Liquid Simulations) and a force field previously used for carbon structures (for more details see [13]). The bonds were constrained by LINCS (LINEar Constraint Solver) algorithm [14] and the Coulomb cut-off [15] scheme with a cut-off distance of 1 nm was applied to account for the Coulomb interactions.

The nanocomposite system consists of one edge-functionalized graphene embedded in an oligomeric PolyEthylene (PE) matrix. Each polyethylene chain contains 11 monomeric units (11-mer, i.e., 22 carbons) and the number of chains in the systems has been adjusted to achieve 3.6 % weight percentage of the graphene nanofiller

in polymer. The size of the graphene sheet is $5 \times 5 \text{ nm}^2$ and its hexagonal lattice made of carbon atoms has been modified on the edges by attaching functional groups, namely either hydrogen or carboxyl groups.

We use the GROMACS [15] simulation package to perform the simulations. The temperature 450 K was kept constant by the stochastic velocity-rescaling algorithm and the Berendsen barostat was applied to maintain the pressure of 1 atm. The time step was 1 fs and a typical production run was about 100 ns long.

B. Coarse Graining Details

In the case of the bulk PE system used for the CG simulation, a first level of CG representation was performed by the use of the united atom approach. Each methyl (CH_3) and methylene (CH_2) group along the chain backbone is treated as one interaction site [12][16]. Nonbonded interactions were described again by the TraPPE force field [12]. The atomistic bulk system consists of 420 chains of 11-mer PE, at 450 K.

In order to produce the CG force field that is consistent with the structure of the atomistic MD simulations, we have used the IBI method. The methodology is based on an iterative numerical minimization procedure having as target the extraction of an effective mean potential that agrees with the atomistic pair distribution function ($\bar{g}^{(ref)}$). The CG potential is refined at each iteration according to following recursive relation [7]:

$$\bar{U}_{eff}^{(i+1)}(r) = \bar{U}_{eff}^{(i)}(r) + ck_B T \ln \frac{\bar{g}^{(i)}(r)}{\bar{g}^{(ref)}(r)}, \quad (6)$$

where c is a constant to ensure the stability of the iteration procedure. The criterion for convergence is whether in each iteration (i) the CG non-bonded distribution function $\bar{g}^{(i)}$ matches the one derived from the atomistic run, within the numerical accuracy. Thus, the two-body potential of mean force, also converges to the (two-body) reference effective potential. The same procedure is also applied for the bonded part of the potential, based on bonded distribution functions.

III. RESULTS AND DISCUSSION

In Figure 2, we present a snapshot of the simulated PE/graphene system in atomistic detail. At the edges of the graphene sheet we may identify the hydrogen and the carboxyl groups. The normalized density as a function of the radial distance from the center of the graphene (data shown in [17]) indicates that at short distances close to 0.5 nm, a peak in the density of PE is present. This is accompanied by an orientation of the polymer chains parallel to the graphene, similar to the behavior observed in different systems [18][19]. At longer distances, as we approach the edges of the nanosheet the density reaches bulk values. The results verify structural heterogeneities.

Concerning the dynamical properties in the nanocomposite system, results based on the AutoCorrelation Functions (ACF) for the case of segmental (1-3 atoms vector) relaxation and the relaxation of the end-to-end vector (at $T=450 \text{ K}$), are presented in Figure 3. The ACFs concern the whole nanocomposite system and confirm the different time scales that govern the relaxation at different length scales. The dynamical heterogeneities are expected to become more pronounced as the temperature decreases reaching values closer to the T_g (220 K [20]), where the diffusion is characterized by increased cooperativity [6].

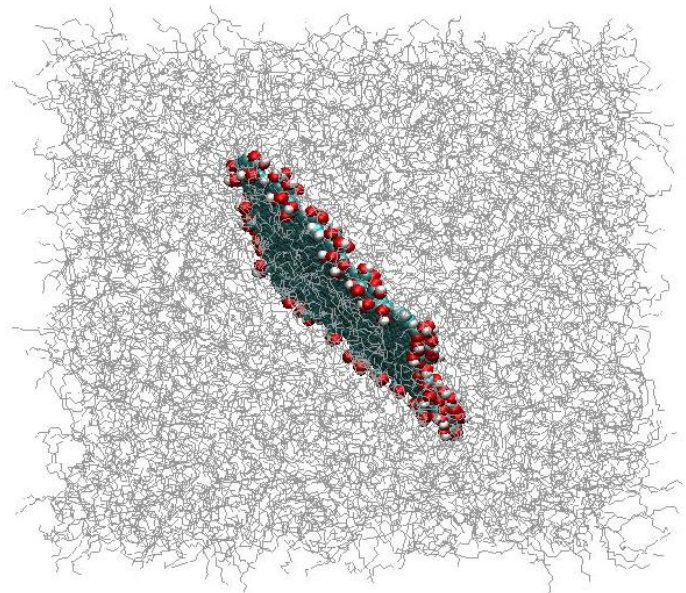


Figure 2. PE/graphene system visualized with VMD [19].

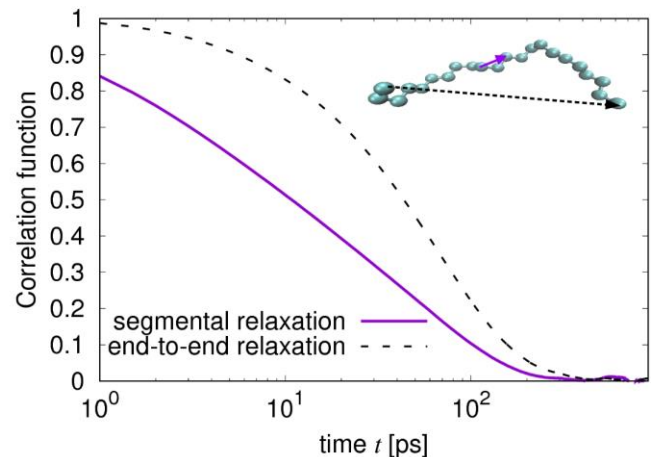


Figure 3. Autocorrelation function of the relaxation of the end to end vector and the segmental bond vectors, at 450K.

By defining the coordination systems of the nanosheet, based on the eigen vectors of the gyration tensor, we can also study the dynamics in different layers from the surface [21]. The layers' definition was based on the minimums in the density profile fluctuations. It is observed that the nanofiller also imposes a distribution in the relaxation times in layers parallel to to the nanosheet, that covers a wide range in the time scale (data shown in [8][21]). The adsorbed layer is characterized by adsorption/desorption times of the order of ms, while the bulk depicts decorrelation times close to ns. Because of this wide spread of time scales CG models could be of great importance.

In order to give a general idea of the CG methodology, here we present new results on a 11-mer bulk PE, focusing on the derivation of the effective PMF for the non-bonded interaction. In Figure 4, we show the chosen CG mapping. Four united atom carbons build a super-atom. The non-bonded pair distribution function of the CG beads, $g(r)$, using the atomistic simulation data, is shown in Figure 5 as "target".

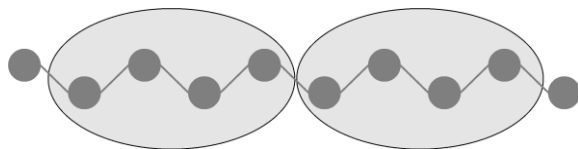


Figure 4. Representation of PE in CG methodology.

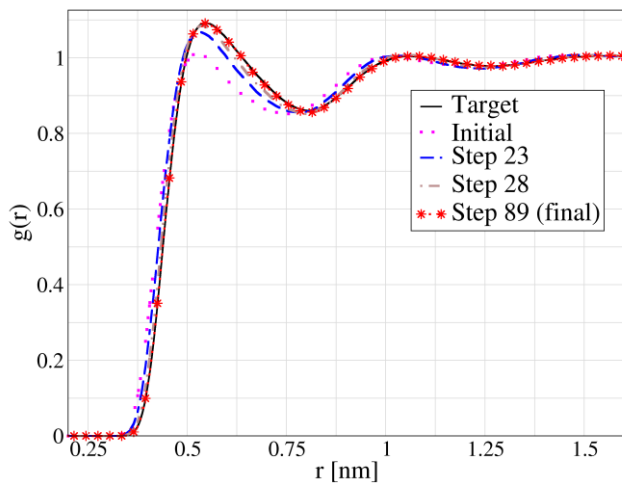


Figure 5. Radial distribution function evolution in the IBI iteration procedure.

Using the IBI method (5), we may determine the non-bonded potential for the CG simulation. In Figure 6, we show the first estimation based on the DBI approach (first iteration), while the evolution of the CG effective potential and respective evolution of the $g(r)$ are depicted by the same kind of lines in Figures 5 and 6. We may conclude that a convergence is succeeded at the 89th step of the iteration.

The final CG effective potential is depicted with asterisks in Figure 6. It consists of a repulsive part at distances lower than 0.6 nm and an attractive part at further distances. A similar procedure is followed for the bonded potentials (not shown).

Structure based CG models using a pair potential usually do not determine adequately the (long-range) attractive part of the effective potential and the virial pressure of the system, as the structure is more affected by the repulsive part of the effective pair potential [3][7]. Incorporation of ideas [6] concerning the temperature dependence of the cohesion energy at the super-Arrhenius region may lead to different approaches in the calculation of the effective potential that could allow the transferability in different temperatures and molecular weights.

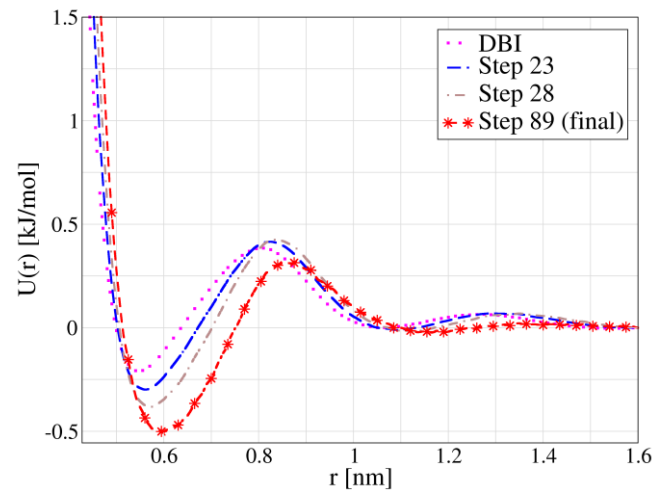


Figure 6. CG effective non-bonded potential evolution. The respective $g(r)$ in each iteration is depicted in Figure 5.

IV. CONCLUSIONS AND FUTURE WORK

In this work we have provided an overview of atomistic and coarse-grained simulations of macromolecular systems. A hierarchical description of such systems requires at the first stage an atomistic description, which was presented for the case of PE/graphene system. We have computed results concerning the structure and the dynamics of polymeric chains at the polymer/graphene interface. The results depict increased structural and dynamics heterogeneities in the nanocomposite system and underline the significance of CG modelling. Derivation of CG potentials that describe the non-bonded interaction were illustrated for the case of bulk PE chains. Moreover, we have presented ideas for the extension of the transferability and predictivity of such methods based on universal characteristics at the super-Arrhenius region.

Current and future work concerns the development of CG models for heterogeneous polymer/particle nanocomposites.

REFERENCES

- [1] K. Johnston and V. Harmandaris, "Hierarchical simulations of hybrid polymer–solid materials," *Soft Matter*, vol. 9, pp. 6696–6710, 2013. doi:10.1039/c3sm50330e.
- [2] W. G. Noid, "Perspective: Coarse-grained models for biomolecular systems," *J. Chem. Phys.*, vol. 139, pp. 090901.00–25, 2013. doi:10.1063/1.4818908.
- [3] D. Rosenberger and N. F. A. Van Der Vegt, "Addressing the temperature transferability of structure based coarse graining models," *Phys. Chem. Chem. Phys.*, vol. 20, pp. 6617–6628, 2018. doi:10.1039/c7cp08246k.
- [4] D. Reith, M. Pütz, and F. Müller-Plathe, "Deriving effective mesoscale potentials from atomistic simulations," *J. Comput. Chem.*, vol. 24, pp. 1624–1636, 2003. doi:10.1002/jcc.10307.
- [5] V. Harmandaris and K. Kremer, "Dynamics of polystyrene melts through hierarchical multiscale simulations," *Macromolecules*, vol. 42, pp. 791–802, 2009. doi:10.1021/ma8018624.
- [6] G. Kritikos and K. Karatasos, "Temperature dependence of dynamic and mechanical properties in poly(acrylic acid)/graphene oxide nanocomposites," *Mater. Today Commun.*, vol. 13, pp. 359–366, 2017. doi:10.1016/j.mtcomm.2017.11.006.
- [7] E. Kalligiannaki, A. Chazirakis, A. Tsourtis, M. A. Katsoulakis, P. Plecháč, and V. Harmandaris, "Parametrizing coarse grained models for molecular systems at equilibrium," *Eur. Phys. J. Spec., Top.* vol. 225, pp. 1347–1372, 2016. doi:10.1140/epjst/e2016-60145-x.
- [8] K. Johnston and V. Harmandaris, "Hierarchical multiscale modeling of polymer–solid interfaces: Atomistic to coarse-grained description and structural and conformational properties of polystyrene–gold systems," *Macromolecules*, vol. 46, pp. 5741–5750, 2013. doi:10.1021/ma400357r.
- [9] W. Tscho, K. Kremer, J. Batoulis, T. Burger, and O. Hahn, "Simulation of polymer melts. I. Coarse-graining procedure for polycarbonates," *Acta Polym.*, vol. 49, pp. 61–74, 1998.
- [10] L. Lu, J. F. Dama, and G. A. Voth, "Fitting coarse-grained distribution functions through an iterative force-matching method," *J. Chem. Phys.*, vol. 139, pp. 121906.00–10, 2013. doi:10.1063/1.4811667.
- [11] T. Schneider and E. Stoll, "Molecular-dynamics study of a three-dimensional one-component model for distortive phase transitions," *Phys. Rev. B.*, vol. 17, pp. 1302–1322, 1978. doi:10.1103/PhysRevB.17.1302.
- [12] N. Lubna, G. Kamath, J. J. Potoff, N. Rai, and J. I. Siepmann, "Transferable potentials for phase equilibria. 8. United-atom description for thiols, sulfides, disulfides, and thiophene," *J. Phys. Chem. B.*, vol. 109, pp. 24100–24107, 2005. doi:10.1021/jp0549125.
- [13] M. G. Martin and J. I. Siepmann, "Transferable Potentials for Phase Equilibria. 1. United-Atom Description of n - Alkanes," *J. Phys. Chem. B.*, vol. 102, pp. 2569–2577, 1998. doi:10.1021/jp972543+.
- [14] B. Hess, H. Bekker, H. J. C. Berendsen, and J. G. E. M. Fraaije, "LINCS: A Linear Constraint Solver for molecular simulations," *J. Comput. Chem.*, vol. 18, pp. 1463–1472, 1997. doi:10.1002/(SICI)1096-987X(199709)18:12<1463::AID-JCC4>3.0.CO;2-H.
- [15] B. Hess, C. Kutzner, D. Van Der Spoel, and E. Lindahl, "GRMACEs 4: Algorithms for highly efficient, load-balanced, and scalable molecular simulation," *J. Chem. Theory Comput.*, vol. 4, pp. 435–447, 2008. doi:10.1021/ct700301q.
- [16] G. Kritikos, A. Sgouros, G. G. Vogiatzis and D. N. Theodorou, "Molecular Dynamics Study of Polyethylene under Extreme Confinement," *J. Phys. Conf. Ser.*, vol. 738, pp. 012012.00–06, 2016. doi:10.1088/1742-6596/738/1/012012.
- [17] P. Bačová, A. N. Rissanou, and V. Harmandaris, "Edge-Functionalized Graphene as a Nanofiller: Molecular Dynamics Simulation Study," *Macromolecules*, vol. 48, pp. 9024–9038, 2015. doi:10.1021/acs.macromol.5b01782.
- [18] M. Gulde, A. N. Rissanou, V. Harmandaris, M. Müller, S. Schäfer, C. Ropers, et al., "Dynamics and Structure of Monolayer Polymer Crystallites on Graphene," *Nano Lett.* vol. 16, pp. 6994–7000, 2016. doi:10.1021/acs.nanolett.6b03079.
- [19] W. Humphrey, A. Dalke, and K. Schulten, "VMD: Visual molecular dynamics," *J. Mol. Graph.*, vol. 14, pp. 33–38, 1996. doi:10.1016/0263-7855(96)00018-5.
- [20] O. Alexiadis, V. G. Mavrantzas, R. Khare, J. Beckers, and A. R. C. Baijon, "End-bridging Monte Carlo simulation of bulk and grafted amorphous polyethylene above and below the glass transition," *Macromolecules*, vol. 41, pp. 987–996, 2008. doi:10.1021/ma071173c.
- [21] K. Karatasos and G. Kritikos, "Characterization of a Graphene Oxide/Poly(acrylic acid) Nanocomposite by means of Molecular Dynamics Simulations," *RSC Adv.*, vol. 6, pp. 109267–109277, 2016. doi:10.1039/C6RA22951D.

Knowledge-Based Decision Support with Self-Learning Methods

Klaus Peter Scherer, Constantin Rieder, Markus Germann
 Institute for Automation and Applied Informatics
 Karlsruhe Institute of Technology,
 Eggenstein-Leopoldshafen, Germany
 e-mail: klaus-peter.scherer@kit.edu
 constantin.rieder@kit.edu
 markus.germann@kit.edu

Joachim Baumeister, Stefan Plehn
 denkbares GmbH
 Würzburg, Germany
 e-mail: joachim.baumeister@denkbares.com
 stefan.plehn@denkbares.com

Abstract - Intelligent systems are available and helpful to support the decision process for diagnostics in complex technical processes. Normally, such a decision support system consists of a knowledge-based module, which is responsible for the real assistance power, given by an explanation and the logical reasoning processes. The knowledge acquisition and generation of the complex knowledge correlations are crucial, because there are different correlations between the complex parameters. So, in this approach, (semi)automated self-learning methods are researched and developed for an enhancement of the quality of such a decision support system.

Keywords – computer-aided assistance; self-learning methods; expert system; decision support; intelligent diagnostics; knowledge base.

I. INTRODUCTION

In the field of diagnostics for complex process behavior, the computer-based assistance is very important and useful. Concerning an enhancement and optimization of the decision making process of the diagnostic experts, there is a need to correlate all information obtained from the available data of the inspected process or system. Ideally, these data sets can be retrieved from the machine facility, the individual components, the functionality and the process parameters. For human beings, it is sometimes impossible to find out hidden knowledge in large data sets. This paper is divided in four sections:

The second section outlines the necessary data and structures as well as technical properties that are important for presented self-learning methods and expert support. The third section describes certain techniques and methods that are used in the approach presented to implement a semi-automated assistance through statistical and self-learning procedures. The last section discusses the results and possible procedures that can significantly support the work of an expert.

II. INFORMATION TECHNOLOGY

In the information technology, knowledge-based methods are predestined to make available both the human expertise and the background deep knowledge to perform the logical

reasoning process [1]. So, the need is to find out a suitable structure to store and manage the heterogeneous distributed knowledge and the expertise of the experts. Furthermore, intelligent self-learning mechanisms can help to enhance the power of the knowledge base.

A. Ontology and Dependencies

On the basic layer, a frame-based information system is performed with all features of the different ontologies. The descriptive layer for the interested information categories is a hierarchical class-subclass system with a refinement process and a special specification from class to subclass.

An ontology concept [2] consists of the declarative part of the semantics, the meaning in this knowledge-based approach, the sources (publications, authors and so on) and multimedia representations (pictures, tables, movies) of the machine components, the parameters and the functionalities. On the next layer, the concept of the semantic dependencies is subdivided into weak and strong types of relations. The knowledge domains of the first layer can be correlated by so called weak links, i. e., semantic associations between the different domains. Considering a selected domain, the diagnostic expert is suggested to also regard the semantic neighbored knowledge domain. However, there exist no strong logical dependencies between the two knowledge items. The human expert can be guided from one point of interest to another in an intelligent manner. An additional type of relation is performed by a stronger relation, such as a rule in a rule based approach. If the premises of the first domain are given, then the second knowledge items result as a conclusion from the preconditions [3].

B. Knowledge Representations

The frames represent the static multimedia information (text, pictures, and audio) including the source information (i.e., HTTP-addresses, literature and links).

The context and the correlations between the different frames are represented as associations, sometimes undirected, sometimes logically directed as implications. This software component is responsible for an intelligent, context sensitive navigation through the knowledge base and the ontologies [4].

tables or lists can be extracted as rule-based representation. This is a real assistance power of the knowledge based decision for the diagnostics in complex technical processes.

ACKNOWLEDGMENT

The research and development of the proposed semi self-learning assistance system is funded by the national economical government of Germany. It is proposed to install a commercial system based on the results of the presented prototype at our industrial partners. The authors thank the project executing organization AiF in Berlin, which is responsible for the allocation of the budget to the research center and the commercial company.

REFERENCES

- [1] R. Studer, R. Benjamins, and D. Fensel, "Knowledge engineering in Principles and methods", in *Data and Knowledge engineering* Vol 25, pp 161-197, 1988
- [2] V. R. Benjamins, D. Fensel, and A. Gomez Perez, "Knowledge management through ontologies", in *Proceedings on the Int. conf. on Practical Aspects of Knowledge Management (PAKM 98)*, Basel, Schweiz, 1998
- [3] K. P. Scherer, "Hypothesis Generation in the context of an ophthalmic application", in *Intern. Conf. on Applied Computer Science*, Genua, Italy, pp 130, 2009
- [4] J. Baumeister, J. Reutelshoefer, and F. Puppe, "Engineering Intelligent Systems on the Knowledge Formalization Continuum", *International Journal of Applied Mathematics and Computer Science (AMCS)*, Vol. 21, 2011
- [5] B. Shneiderman, "The eyes have it: a task by data type taxonomy for information visualizations", in *Proceedings of the IEEE Symposium on Visual Languages*, pp. 336 – 343, 1996
- [6] M. Atzmueller, and F. Lemmerich, "VIKAMINE – Open-Source Subgroup Discovery, Pattern Mining, and Analytics", in *Proceedings of the European Conference on Machine Learning and Principles and Practice of Knowledge Discovery in Databases*, Heidelberg, Germany, 2012

An Innovative Crowd Segmentation Approach based on Social Force Modelling

Yu Hao^{1,2}, Zhijie Xu², Ying Liu¹, Jing Wang³, Jiulun Fan¹

Xi'an University of Posts and Telecommunications¹, University of Huddersfield², Sheffield Hallam University³
Xi'an, China¹, Huddersfield, UK², Sheffield, UK³

E-mails: haoyu@xupt.edu.cn, z.xu@hud.ac.uk, ly_yolanda@sina.com, jing.wang@shu.ac.uk, jiulunf@xupt.edu.cn

Abstract—The effective segmentation and separation of groups in a crowd serves a crucial role in the video analysis for crowd behavior understanding. Conventional crowd segmentation techniques rely on the spatial distribution or temporal trajectories of individual agent in the crowd. However, psychological influences among subjects in a high density crowd are often ignored. In this research, an enhanced Social Force Model (SFM) is developed to define in-crowd motions among agents and its affiliated groups. An innovative SFM descriptor - the Grouping Center - is modeled as a key feature for aiding accurate crowd segmentation. During the process, extracted optical flows are mapped to the detected agents, then the SFM components such as the desired force and the repulsive force are calculated. Experiments show accurate segmentation can be achieved even when agents from different groups are heavily (spatially) mixed up. Random crowd scenarios generated by a commercial game engine are used for crowd behavior analysis and model evaluation. Evaluations indicate that the new SFM model and its related-techniques are capable of handling complex crowd scenarios with latent semantic meanings.

Keywords- crowd segmentation; motion prediction; social force model.

I. INTRODUCTION

The analysis of crowd behaviors is becoming a crucial research issue to support the maintenance of public safety. With the wide installation of Close Circuit Television Inspection (CCTV) cameras in public area, the massive amount of recorded video data could be exploited for the prediction of potential danger, real-time anomaly alerts and forensic evidences. The segmentation of the crowd in video data usually serves as the pre-processing stage in the framework of crowd analysis, yet it is a vital component of the entire pipeline. The precise segmentation of the crowd would have significant influence on the performance of feature extraction, model training and behavior recognition.

The technique of Crowd Segmentation [1][6] usually consists two fundamental procedures, which are Individual Detection and Motion Prediction. The aim of Individual Detection is to verify as many agents from the crowd as possible. In most crowded videos, the density of the crowd is high. The high density will cause the difficulty to maintain the accuracy of individual detection, for example the issue of frequent occlusion will make the tracking and locating of the pedestrian extremely difficult. In order to address this issue, approaches of individual detection under heavy occlusion are proposed by various researches [1]-[7]. Some other segmentation approaches attempt to consider the crowd as a single entity to avoid the individual detection. By analyzing the flow-based information of this entity, the crowd is segmented according to its spatial and temporal relationship. However, this kind of approach is not capable

of handling the following situation. Assuming agents with two different destination are randomly distributed, the approach cannot segment these agents into two groups until they are spatially separated, or the temporal information such as trajectory are calculated after some amount of time. In order to achieve the successful segmentation of these two groups in the early stage, this research devised a segmentation approach based on Individual Detection and the concept of Social Force. This approach will be able to segment the randomly distributed crowd according to the proposed Group Attraction Force. The detailed algorithm will be introduced in following section. The aim of Motion Prediction is to predict the long-term behaviors of detected individuals according to their spatial and temporal information. In the procedure of Motion Prediction, states such as position and trajectory are fed to a behavioral model to estimate the individual's next motion. Once the long-term behavior of each detected individual is obtained, a classifier could be implemented to cluster the estimated behavior for the segmentation of the crowd.

The techniques of individual detection consist of two approaches. In the first approach, the statistical or shape information is extracted from the image and feed to the trained classifier for the detection result [1]-[5]. In the second approach, a rough estimation such as head/shoulder detector is implemented to generate hypotheses. Then the concept of Expectation Maximization (EM) is exploited to verify these hypotheses based on various iterations [6][7].

In the research of Lan [1], the image is firstly preprocessed into a foreground image. Then the silhouette of the foreground image is sampled and transformed with Discrete Fourier Transform as a Fourier Descriptor. The silhouette can be reconstructed anytime with Fourier coefficients. The Euclidean distance between two Fourier Descriptors is utilized to measure the similarity of silhouettes. Next, KNN and locally-weighted regression are used to find the closest match of target image among the trained sample sets. The machine learning techniques are frequently utilized as well in recent researches. Kang [3] mentioned for crowd with high density, appearance-based approaches with patterns such as HOG, Scale-invariant feature transform (SIFT) and Linear Binary Pattern (LBP) do not have good performance. Techniques of Deep Learning are widely implemented in computer vision field. In the research, the so-called Fully Convolutional Neural Network (FCNN) is used for crowd segmentation with both appearance and motion features. In the FCNN, a multiple stage deep learning architecture with features of appearance, motion and structure is devised. In this research, the FCNN claims to have advantages than the conventional CNN.

In the research of Tu [6], the concept of EM is utilized to verify the segmentation hypothesis, and it attempts to

achieve the correct detection under serious occlusion situation. In the first step of this approach, a rough head and shoulder detection are applied on the image, each detected pedestrian is named hypotheses. However, due to the complexity of scene and the occlusion problem, many false positive detections will occur. For the second step, the image is divided into a grid of patches. Next, this research proposed an algorithm to calculate the so-called Affinity between each patch and hypotheses. In order to further optimize the segmentation hypotheses, the concept of EM is imported to address this issue. An approach with similar methodology, but different details is proposed in [7]. In this approach, a scale-invariant interest point operator [8] is firstly used to locate the Points of Interests. Around these points, patches with certain radius are extracted from the image. Next, an agglomerative clustering scheme [9] is implemented on each patch to obtain a representation of its structure as the signature for the hypothesis's verification. Then the spatial occurrence distribution is used to measure the distance between different signatures. For each iteration of the E-step, patches are extracted from the interest points, and the distance is measured by the trained codebook using spatial occurrence distribution to verify the hypotheses. And for the M-step, the measured result will be used to update the codebook. After several iterations, the updated hypotheses are recognized as detected pedestrians.

With the premise of well devised agent behavioral model and successfully detected agent motion state, it is expected to have an accurate prediction of agent's next movement. However, in real-life cases, this premise is very difficult to fulfill. It will make conventional motion prediction approaches do not show a satisfying performance in real-life scenario. Furthermore, the conventional approach is only capable of making the prediction of short-term movement. As long as the approach is applied to the longer-term prediction, the accuracy decays drastically. In order to address this issue, two alternative approaches are proposed by the following researches. 1) Instead of detecting the motion state of an agent, a grid is placed onto the current image. For each cell within this grid, the transition probability is calculated for an agent moving to next cell [10] [11]. 2) All trajectories inside scene are firstly detected. Then trajectories with similar patterns are clustered. The clustered trajectory will be used for prediction of next motion [12] [13].

The Social Force Model [15] is primarily implemented in the field of crowd simulation, and sometime crowd analysis. In most of the segmentation algorithm, spatial information such as co-ordinate, size and shape, temporal information such as trajectory are exploited. However, the behavior of pedestrians within highly dense environment could be easily influenced by the psychological factor with its neighbors. In this research, the Social Force Model along with the improved concepts such as personal space and perception field are utilized to devise an innovative signature for crowd segmentation namely Grouping Center. The result of following experiments indicates the segmentation approach with psychological concept is capable of handling the mixed crowd from multiple groups.

The structure of this contribution is composed as follows. Section 2 gives a detailed introduction of the

proposed crowd segmentation approach. To be specific, the innovative concept of Group Attraction Force is explained and the extraction algorithm is introduced. In Section 3, the proposed algorithm is formulated to achieve a more explicit explanation. In Section 4, the proposed approach is implemented on the simulated crowd video to assess the performance of segmentation. Section 5 provides the conclusion and discusses the future work.

II. CROWD SEGMENTATION APPROACH AT HIGHLY MIXED STATE

In the previous work [14], a simulation model based on the Social Force Model (SFM) is devised to generate crowd behavior with visual realism. The concept of SFM is firstly proposed by Helbing [15], and widely exploited on crowd simulation and behavioral modeling. The fundamental concept of SFM is the motion of every pedestrian among the crowd is affected by three types of psychological-related forces: Desired Force, Repulsive Force and Avoidance Force, which is formulated as (1). Which sf_i is the final force determines the motion of pedestrian i . f_d is the desired force, f_{ji} is the repulsive force from neighbor j , and f_{oi} is the avoidance force from obstacle o .

$$sf_i = f_d + \sum_{j \neq i} f_{ji} + \sum f_{oi} \quad (1)$$

In the proposed simulation model, an innovative group attraction force is devised to achieve a better visual realism of the simulated crowd. In the simulation scenario, sixty agents from three different groups are randomly distributed on the stage. Each agent is mapped with a behavioral model which controls the agent's motion. The behavioral model contains parameters such as personal space, radius, angle of perception. The radius describes the size of each agent. The personal space and angle of perception determine the repulsive force affected on the agent. If a neighboring agent exists in the range of personal space and perception angle, the repulsive force will be generated, otherwise it will be omitted. In order to further increase the visual realism, based on the assumption that simulated agents always attempt to stay closer to the cluster with agents from same group, the concept of Group Attraction Force is devised to enhance the conventional SFM. To model the Group Attraction Force, agents with same group number appeared in the perception field of current agent are firstly allocated. Then the average position of the allocated agents is calculated as the Grouping Center. Next, a force from current agent to the grouping center will be estimated as the Group Attraction Force. The simulation result shows the group attraction force embedded behavioral model presents the better performance than the conventional SFM on the visual realism. The enhanced SFM with Group Attraction Force could be adjusted as in (2), in which f_{Gi} is the Group Attraction Force.

$$sf_i = f_d + \sum_{j \neq i} f_{ji} + \sum f_{oi} + f_{Gi} \quad (2)$$

By further investigating the distribution of Grouping Center, it could be observed that despite the spatial distribution of agents from three different groups is sparse and random, the Grouping Centers from different groups are naturally clustered. As illustrated in Fig. 1(a), the spatial

distribution of agents is very random. It is almost impossible to use classifiers such as KNN to segment. However, according to the Group Attraction Force Model, the calculated distribution of group centers exhibits significant patterns, as illustrated in Fig. 1(b). The Fig.1(c) shows the distribution of grouping centers in large scale. It could be explicitly observed that grouping centers are naturally clustered.

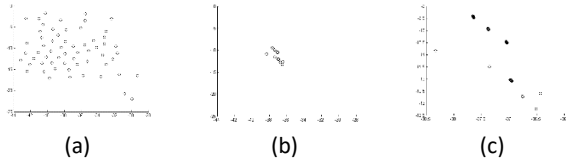


Figure 1. The comparison of distribution between spatial position and group center. (a) Spatial distribution. (b) Grouping center distribution. (c) Magnified grouping center distribution

Upon this observation, it is worthy to try segmenting agents according to the clustering result of group centers. Therefore, the simple KNN clustering algorithm is exploited for the segmentation. It's assumed that the value of K is correctly determined, in this case K equals to 3. As illustrated in Fig. 2(a) shows the Ground Truth spatial distribution of agents from three different groups. Agents from same group are labeled with same shape. Fig. 2(b) shows the segmented result using proposed approach. In this case, 53 out of 60 agents are correctly segmented comparing to the ground truth.

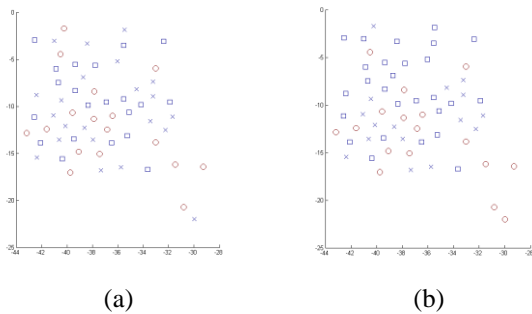


Figure 2. Comparison between ground truth and segmentation result. (a) Ground Truth. (b) Segmentation Result using Grouping Center

The previous paragraphs proved that the Grouping Center is capable of segmenting crowd consists of multiple groups at randomly distributed state. In order to exploit the Grouping Center to achieve desired segmentation performance, a fundamental issue still needs to be addressed. In the previous paragraph, it is assumed that agent knows the group number of other agents. Based on this assumption, the Grouping Center could be calculated. Nevertheless, in the process of segmentation on the crowd video obtained from the CCTV cameras, the group number of each pedestrian is unknown. Thus, the Group Centers for pedestrians cannot be obtained directly. Therefore, an innovative algorithm to estimate Group Attraction Force from two consecutive frames is introduced. The architecture of the algorithm is illustrated in Fig. 3.

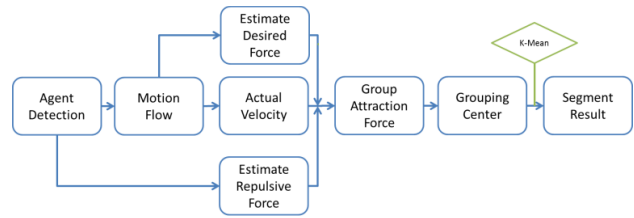


Figure 3. The framework of the proposed crowd segmentation approach

For each agent, the group attraction force f_{Gi} is unknown. if the actual force sf_i , desired force f_d , repulsive force $\sum_{j \neq i} f_{ji}$ and avoidance force $\sum f_{oi}$ are obtained, the group attraction force could be calculated according to (2). With the obtained group attraction force, the Grouping Center will be calculated.

In the procedure illustrated in Fig. 3, every agent needs to be detected at the first step using the main stream pedestrian detection algorithm such as [3]. For each detected agent, the parameters of SFM such as personal space, radius and angle of perception are estimated according to the current environment. The radius of agent could be estimated upon the average pixel number of all detected agents. Once the radius is determined, the personal space could be decided empirically. The angle of perception could be set to the same value of the simulation model. Therefore, the repulsive force $\sum_{j \neq i} f_{ji}$ of all detected agents i could be calculated.

On the other hand, the global flow-based information between two consecutive frames is extracted, and mapped to each agent. The flow-based information such as optical flow could be transformed into the actual velocity of mapped agent and set as the actual social force sf_i . The estimation of desired force f_d could be a difficult task, since the group number of current agents is unknown. Therefore, the destination cannot be determined. In order to address this issue, several constrains have been made to simplify the problem. Firstly, agents are assigned into two groups. The destinations of these groups located at opposite directions on the scene. Secondly, if the actual force of agent is large enough, the direction of desired force is identical to the actual force, since the magnitude of repulsive and group attraction force are usually much smaller than the desired force. Thirdly, if the actual force is not large enough, it will be close to the repulsive force. In this case, the direction of agent's desired force will be randomly determined. Considering the complexity of scenario, the avoidance force $\sum f_{oi}$ is omitted. In the following experiment, the scene only consists with floor, agents and destination. The obstacle is removed from scene.

With the estimated desired force, repulsive force and actual social force, the group attraction force could be estimated according to (2). Since the group attraction force is a vector, the grouping center could be calculated using current position of the agent. With the estimated grouping centers, the conventional classifier such as KNN could be utilized to segment the crowd.

In next section, the proposed algorithm is formulated in order to help better understanding the proposed approach.

III. FORMULATION OF THE PROPOSED APPROACH

According to the framework introduced in Fig. 3, the group attraction force f_{Gi} of agent i could be derived from the (2). As explained in previous section, the avoidance force is omitted in order to simplify the model. The estimated group attraction force f_{Gi} of agent i is presented as (3).

$$f_{Gi} = sf_i - f_d - \sum_{j \neq i} f_{ji} \quad (3)$$

in which sf_i is the actual social force obtained from the optical flow information. f_d is the estimated desired force, the magnitude of f_d is a constant α , and its direction could be presented as (4).

$$\text{dir}(f_d) = \begin{cases} \text{dir}(sf_i) & \|sf_i\|_2 > \tau \\ \theta & \text{otherwise} \end{cases} \quad (4)$$

where τ is a threshold constant, if the magnitude of actual force sf_i is greater than the threshold τ , the estimated direction of f_d will be same as actual force. Otherwise, the direction of f_d will be randomly determined between two goals.

The calculation of actual force sf_i , is based on the flow-based information. In this research, the conventional Horn Schunck optical flow patterns [17] are first extracted from two consecutive frames. Next, the standard pedestrian detection algorithm is applied to obtain the position of each agent. By mapping the optical flow to each agent, the actual force could be determined. The actual force sf_i could be represented as (5).

$$sf_i^{x,y} = \sum k f_o^{x \pm 1, y \pm 1} \quad (5)$$

where $sf_i^{x,y}$ is the actual force of agent i at position xy , $f_o^{x \pm 1, y \pm 1}$ is the optical flow vector on position xy , k is the weight factor, when $x=0$ and $y=0$, $k=1$, otherwise $k=0.4$ in this case.

The calculation of repulsive force f_{ji} is imported from Qingge's Velocity Perception Based SFM [16]. In the conventional SFM, the repulsive force is set as a constant magnitude value β . If the distance between current agent and any neighboring agents is less than personal space ρ , the repulsive force will be applied to the agent, otherwise no repulsive force will be applied. This solution will generate the significant 'vibration' phenomenon between agents. Instead of using a constant value, (6) is devised to describe the most realistic repulsive force between agent i and j .

$$f_{ji} = A_i e^{(r_{ij} - d_{ij})/B_i} n_{ij} \quad (6)$$

where A_i and B_i are the constant values to control the magnitude scale of the repulsive force. r_{ij} is the sum of two agents' radius. d_{ij} is the distance between two agents. The exponential function ensures the fast dispersing when the distance between two agents increase and vice versa. n_{ij} describes the direction of the repulsive force. In order to further increase the realism of simulated repulsive force, the personal space ρ and perception field are also considered. The extracted repulsive force is further regulated using (7). If the distance between two agents is

smaller than the summation of agent i 's personal space and agent j 's radius, the repulsive force remains the same. Otherwise the repulsive force equals to zero when the distance between two agents is not in the range of the personal space.

$$f_{ji} = \begin{cases} f_{ji} & d_{ij} \leq \rho_i + r_j \\ 0 & \text{otherwise} \end{cases} \quad (7)$$

Even if the distance satisfied the range of personal space, the perception of agent and the motion direction could still need to be specifically modeled. In real-life, the repulsive force exhibits different patterns on three different circumstances. While two agents are moving along similar direction, the agent in the front should not be affected by the repulsive force from the one behind. While two agents are moving along opposite direction and about to collide, they should be both affected by the repulsive force. While two agents are moving along opposite direction but back to back, both of them should not be affected by the repulsive force. According to these details, the repulsive force f_{ji} could be further constrained using (8).

$$f'_{ji} = \begin{cases} \theta((v_j - v_i)n_{ij})G_{ij}f_{ji} & d_{ij} > \rho_i + r_j \\ (1 + \theta((v_j - v_i)n_{ij})G_{ij})f_{ji} & d_{ij} \leq \rho_i + r_j \end{cases} \quad (8)$$

where $\theta(z)$ equals to zero if $z < 0$, and equals to z otherwise. The range of G_{ij} is from 0 to 1, which is used to impact the magnitude of repulsive force when two agents are moving along opposite directions.

With the proposed equations, the Group Attraction Force f_{Gi} of agent i could be estimated. Since f_{Gi} is a vector, the co-ordinate of Grouping Center could be finally obtained using f_{Gi} and agent i 's co-ordinate (x_i, y_i) .



Figure 4. A snapshot of the simulated video

IV. EXPERIMENTAL SETTINGS AND RESULTS

The video data used for experiment is generated by 3D game engine Unity. The scene is composed with 40 agents, and each agent is replaced with a sphere for easier individual detection. Agents are assigned to two different groups, 20 agents for each. Agents from different groups are mapped with different textures. As illustrated in Fig. 4, agents from group 1 are mapped with dark green color and those from group 2 are mapped with bright white color. The two hexagons mark destinations of these two groups, agents from group 1 attempt to move toward to the upper destination and agents from group 2 to the lower one. Each

agent in the stage is mapped with a behavioral model consists of the desired force, repulsive force and group attraction force strictly defined using previously proposed formulations.

Fig. 4 illustrates the randomly distribution of two groups. Agents from both groups are mixed up. It's very difficult to segment the crowd in current state using spatial information. According to the architecture of the proposed segmentation procedure in Fig. 3, the first step is to extract the optical flow using the Horn Schunk algorithm. In the experiment, frames of number 20 and 22 are selected for the optical flow extraction. The reason of using the early frames is that agents at this time are still in randomly distributed state. Since the distribution of agents would quickly become clustered under the impact of the group attraction force. The reason of skipping one frame instead of using two consecutive ones is to ensure the magnitude of extracted optical flow is large enough. Because if the magnitude is too small, the optical flow field would be easily affected by factors such as deviation and noise. Fig. 5(a) illustrates the extracted HS optical flow field from Fig. 4. In this experiment, the grid size is set to 10 pixels. Since the ultimate goal of this research is to achieve real-time detection, the overly condensed sampling grid would have the chance to affect the performance of the system. It is necessary to declare that the magnitude of the optical flow is amplified by 3 times to provide a better visual experience. However, the actual motion of each agent is not as drastic as the figure shows.

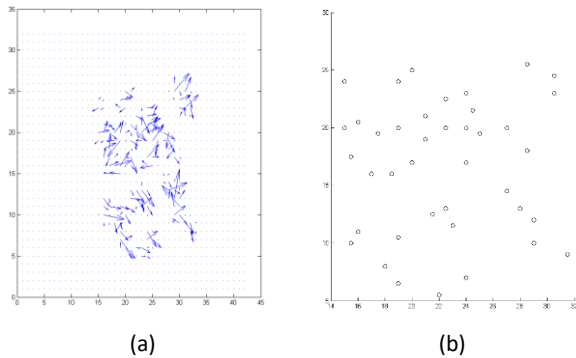


Figure 5. The extracted optical flow and detect agents. (a) The extracted optical flow field using frame 20 and 22. (b) The spatial distribution of detected agents

According to the framework proposed in Fig. 3, agents in the scene need to be correctly detected. In most of the case, conventional people detectors could satisfy the requirement unless the crowd density is too high. Since the agent is represented with a sphere, shape detection algorithm such as Hough Circles could be more reliable. The agent detection result is illustrated in Fig. 5(b).

Next step of the procedure is to map the detected agents with extracted optical flow field to obtain the actual social force. According to the equation (5) proposed in previous section, the average of all nine neighboring optical flow vectors is exploited as the final optical flow for current agent, and the parameter K is still set to 0.4. The obtained actual social forces are illustrated in Fig. 6(a). By comparing the detected agent's motion with the group truth, most behaviors of the agent are basically matched, despite with some deviations.

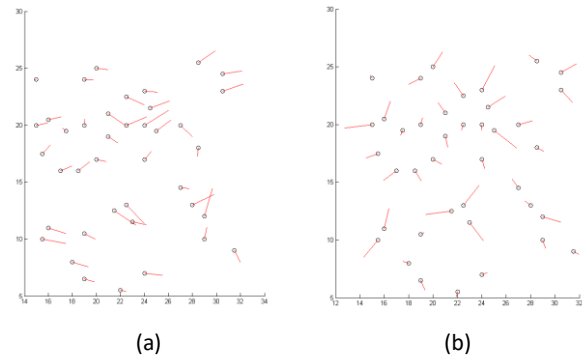


Figure 6. (a) The mapping result of actual social force. (b) The estimated repulsive force

In next step, the repulsive force of each agent is calculated according to (7)(8) and (9). The estimation result of the repulsive force is illustrated in Fig. 8. In this case, the value of personal space ρ is set to 5 pixels, radius of agent r is set to 0.5 pixel. The value of parameter A_i and B_i should be 2 and 0.5. In Fig. 6(b), the value of B_i is set as 1 for a better visual presentation, the actual calculation would still be using 0.5.

Fig. 7 illustrated the estimation result of desired force of each agent. In the experiment, it is assumed the two destinations are successfully detected using Points of Interest detection techniques. Therefore, the only estimation in this step is to determine which destination the agent belongs to using (4). In the experiment, the magnitude of the desired force is set to the average amount of actual force affected from agents.

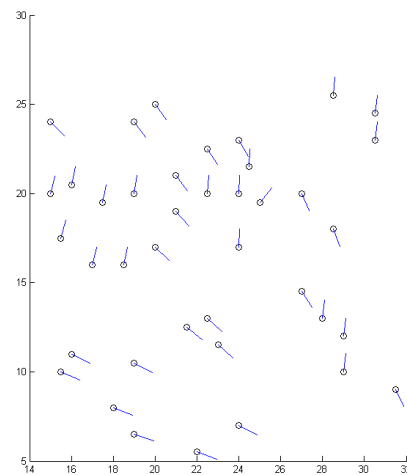


Figure 7. The estimated desired force

Once the actual force, repulsive force and desired force are extracted, the final Group Attraction Force could be estimated with (3). According to the definition of Group Attraction Force, the Grouping Center of each agent could be calculated. Next, the ordinary classifier is applied to the grouping center for the clustering. The clustering result is illustrated in Fig. 8. Agents from different groups are marked with different labels. Comparing the ground truth illustrated in Fig. 4, most of agents are correctly segmented. The accuracy is 87.5% in this example.

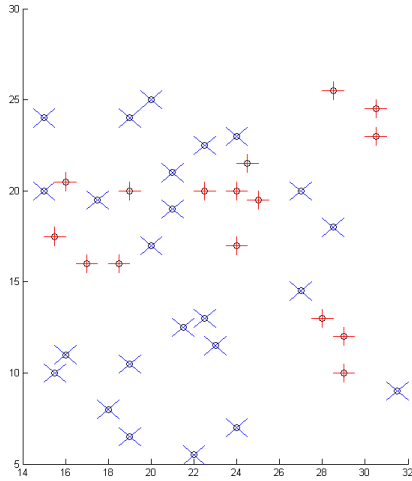


Figure 8. The segmentation result using the proposed approach

V. CONCLUSION AND FUTURE WORKS

In order to achieve effective crowd segmentation under complex sub-grouping states, an innovative Social Force Model is devised in this research. It is based on the assumption that crowd agents from the same behavioral/action group, i.e. a family unit, would make due effort to stay close within a crowd. A novel interaction force, named Group Attraction Force, is devised to populate the SFM feature set for accurately describing crowds formed by sub-groups. The concept of Grouping Center can effectively aid crowd segmentation even when agents from different groups are heavily mixed up.

Unlike conventional crowd segmentation techniques that often rely on spatial and temporal patterns only, the proposed SFM approach achieves superior results with improved semantic interpretation. Random crowd scenarios generated by a commercial game engine are used for crowd behavior analysis and model evaluation. Experiments show accurate segmentation can be achieved even when agents from different groups are heavily (spatially) mixed up. Future work will see test and evaluations being performed on real-life video feeds when factors such as occlusions and illumination variations need to be considered.

TABLE I. PARAMETER SETTING

Parameter Name	Parameter Value
weight factor k	0.4
Relax parameter G_{ij}	0.5
Frames selection	20 and 22
Grid size in optical flow	10 pixels
personal space ρ	5 pixels
radius of agent r	0.5 pixel
A_i	2
B_i	0.5

ACKNOWLEDGMENT

This research is sponsored by Chinese National Natural Science Foundation No. 61671377, and Shaanxi Smart City Technology Project of Xianyang No.2017k01-25-5

REFERENCES

- [1] L. Dong, V. Parameswaran, V. Ramesh, and I. Zoghalmi. "Fast Crowd Segmentation Using Shape Indexing". In 2007 IEEE 11th International Conference on Computer Vision. pp. 14-21. 2007
- [2] N. Dalal and B. Triggs. "Histograms of Oriented Gradients for Human Detection". In International Conference on Computer Vision Pattern Recognition, pp. 886-893. 2005.
- [3] K. Kang and X. Wang. "Fully Convolutional Neural Networks for Crowd Segmentation". In arXiv:1411.4464v1 [cs.CV]. 2014
- [4] N. Dalal and B. Triggs. "Histograms of Oriented Gradients for Human Detection". In International Conference on Computer Vision Pattern Recognition 2005, pp. 886-893. 2005.
- [5] P. Sinha. "Object Recognition via Image Invariants: A Case Study". In Investigative Ophthalmology and Visual Science. Volume 35, pp. 1735-1740. 1994.
- [6] P. Tu, T. Sebastian, G. Doretto, N. Krahnstoeber, J. Rittscher, and T. Yu. "Unified Crowd Segmentation". In Computer Vision - ECCV 2008. Lecture Notes in Computer Science, vol. 5305. Springer, Berlin, Heidelberg. 2008
- [7] B. Leibe, E. Seemann, and B. Schiele. "Pedestrian Detection in Crowded Scenes". In 2005 IEEE Computer Society Conference on Computer Vision and Pattern Recognition (CVPR'05) (2005). San Diego, California, pp. 878-885, June 2005
- [8] D. Lowe. Distinctive image features from scale-invariant keypoints. IJCV, 60(2). pp. 91-110, 2004.
- [9] B. Leibe, A. Leonardis, and B. Schiele. Combined object categorization and segmentation with an implicit shape model. In ECCV'04 Workshop on Stat. Learn. in Comp. Vis., pp. 17-32, 2004
- [10] K. Tanaka, "Detecting collision-free paths by observing walking people," in Proceedings of the 2002 IEEE/RSJ International Conference on Intelligent Robots and Systems, Lausanne, Switzerland, pp. 55-60, 2002.
- [11] S. Tadokoro, M. Hayashi, Y. Manabe, Y. Nakami, and T. Takamori, "Motion planner of mobile robots which avoid moving human obstacles on the basis of stochastic prediction," in IEEE International Conference on Systems, Man and Cybernetics, pp. 3286-3291, 1995.
- [12] S. Gaffney and P. Smyth, "Trajectory clustering with mixtures of regression models", in 99 Proceedings of the fifth ACM SIGKDD international conference on Knowledge discovery and data mining, University of California, Irvine. pp. 99-15, 1999.
- [13] M. Bennewitz, W. Burgard, and S. Thrun, "Learning motion patterns of persons for mobile service robots," in Proceedings of the 2002 IEEE/RSJ International Conference on Intelligent Robots and Systems, pp. 3601-3606, 2002.
- [14] Y. Hao, Zhijie Xu, Ying Liu, Jing Wang, and Jiulun Fan. "Crowd Synthesis Based on Hybrid Simulation Rules for Complex Behaviour Analysis". In Proceedings of the 24th International Conference on Automation & Computing, in press.
- [15] H. Dirk, and P. Molnar. "Social force model for pedestrian dynamics", Physical review, E 51, no. 5, 4282. 1995.
- [16] Q. Ji, F. Wang, and T. Zhu, "VPBS: A Velocity-Perception-Based SFM Approach for Crowd Simulation", In 2016 International Conference on Virtual Reality and Visualization. Hangzhou, China. 2016
- [17] B. Horn, and B. Schunck. "Determining optical flow". Artificial Intelligence, vol 17, pp. 185-203. 1981

Speeding Up the Recommender Systems by Excluding the Low Rated Items

Yousef Kilani

Faculty of Prince Al-Hussein Bin Abdallah II for Information Technology, Hashemite University,
Zarqa, Jordan

Email: ymkilani@hu.edu.jo

Abstract—Recommender systems (RSs) have become an important tool to help users in searching for their favorite items in many real life applications. A Collaborative Filtering is a commonly used technique in RS. In order to recommend items to the active user (the user we want to make recommendation for), collaborative filtering-based RS uses similar users to the active user and/or latent factor techniques. In our project, we show that excluding the items I that have not been rated high by any user speeds up the recommendation process and gives better accuracy, precision, and recall. The RSs recommend the items that have been rated high by the similar users to the active user. No item from I has been rated high by the similar users and, hence, will not be recommended to the active user. As far as we know, there is no similar work in the literature.

Keywords—collaborative filtering; recommender systems; speed; low rated items.

I. INTRODUCTION

Recommender systems (RSs) reduce the time users spend while choosing an item in a supermarket, shopping mall, movie shops, songs shops, travel agency, a book in book store etc. While selecting any item, people usually ask others who chose an item from the same category for a recommendation. Currently, the number of items in any category is increasing tremendously and the user has more and more number of choices which makes him confused of which item to choose. Currently, the fast increase of Web 2.0 has led to the proliferation of collaborative websites in which the number of elements that can be recommended (e.g., blogs) can increase significantly when introduced (and not voted) by the users, which generates new challenges for researchers in the field of RSs [1]. RSs are currently being applied in many different domains [2]. Because of the great importance of RSs, it is interesting to note that an improvement of 10% recommendation accuracy was awarded with 1 million US dollars [3]. Applications of RSs include: DVD rental provider Netflix [4], the online book retailer Amazon [5], Album Advisor [6], the advisor at the Drugstore [7], the RS for the purchase in eBay [8], an e-learning context [9], e-commerce [10], music recommendation [11], healthcare [12], document recommendation [13][14], stock prediction in the PredictWallStreet company [15], recommending personalised news [16] and e-government [17].

The unnecessary items are the items which have not been rated high by any user. In this research, our interest is in speeding up the RSs by obtaining better precision, accuracy, and recall by excluding the unnecessary items. If the active user A is similar to user B , then the Collaborative Filtering

(CF)-based RSs recommend the items to B which have been rated high by A . In other words, the RS will not recommend the items which have not been rated high by user A .

The rest of this paper is organized as follows. We start by introducing the RSs in Section II followed by Section III which shows the related work. Section IV presents our new idea. We incorporate our idea into the Navgaran et al.'s algorithm [18] and we show experimentally the results of the new algorithm using MovieLens dataset in Section V. The last section gives the concluding remarks.

II. THE RECOMMENDER SYSTEMS

We can categorise RSs based on the filtering methods into four categories: collaborative [19], content [3][20][21], demographic filtering [22], and hybrid [23][24]. Kilani et al. [25] mentioned that, currently, CF is probably the most known and commonly used recommendation approach in RS [26]. CF is an excellent method for recommendation systems and its core scheme is to calculate the relation among the products and users based on preferences [27]. Two users are similar if they rated a set of items nearly the same.

The CF-based RSs uses either the Neighbourhood (NM) [28] or the Model (MM) [29] methods. In the NM, the RS makes recommendation for the active user by finding the users who are similar to this user and then recommending the items which were rated high by these users. The user-based CF RS assumes that if two users A and B rated a set of items similarly and A rated a set of other items, x , high then most probably B will rate x also high. Hence, this RS recommends x for B . In the MM, the RS uses the models to recommend items for the active user. The models learn using supervised or unsupervised learning methods to make recommendation. Examples of these models are: Bayesian hierarchical, clustering, and Latent Factor (LFM). Kilani et al. [25] mentioned that Matrix Factorization (MF) methods have recently received greater exposure mainly as an unsupervised learning method for latent variable decomposition and dimensionality reduction [29].

Lu et al. [30] mentioned that content-based RSs try to recommend items similar to those a given user has liked in the past [31]. These RSs compare between the content of the items the active user rated high and the new items which are considered for recommendations. They then recommend from the new items, those that are most similar to the items which have been rated high by the active user.

The demographic-based RSs recommend items for the active user based on the demographic data like: age, gender,

race, place, material status, education level, etc. This data can be leveraged to power the RSs and hence to improve the accuracy of these RSs.

The hybrid RS merges any two or three techniques of the previous three categories (for instance, see [23][24][30]). Kilani et al. [25] mentioned that MF methods have recently received greater exposure mainly as an unsupervised learning method for latent variable decomposition and dimensionality reduction [29].

III. RELATED WORK

This section presents the related works that have been done to speed up the RSs.

Boim [32] built new techniques to boost CF based RS. Boim focuses on four challenges: improving the quality of the prediction, creating new methods to choose items from the recommended items to the user, improving the efficiency of the CF algorithms and related data structures, and incorporating recommendation algorithms in different application domains.

Bachrach et al. [33] introduced a novel order preserving transformation in order to match the inner product between the active user and the items in the matrix factorization technique to Euclidean space nearest neighbor search problem. Our final solution is based on a novel use of the Principal Component Analysis (PCA)-Tree data structure in which results are augmented using paths one hamming distance away from the query (neighborhood boosting). The end result is a system which allows approximate matches (items with relatively high inner product, but not necessarily the highest one) [33].

Formoso et al. [34] showed how compression techniques using coding techniques from Information Retrieval reduces the size of the rating matrix (up to 75 %) and hence speed up (almost doubling) recommendations.

IV. PROPOSED METHOD

This section presents the details of our proposed method. Each user gives a rate of 1, 2,..., or 5 to any item in the system. The higher the value indicates that the user prefers this item more; 1 is the lowest and 5 is the highest. Our idea states that the RS recommends items that have been rated high by similar users to the active user. Therefore, if an item has not been rated high by any user, including the similar users, then no need to consider this item in the recommendation process. This improves the RSs' accuracy. We show in Section V that we may exclude the items which has not given any rate greater than 2, 3, 4, or 5. Our idea can be implemented by any RS.

V. EXPERIMENTS

We have incorporated our idea into the Navgaran et al.'s algorithm [18] (NA). We have chosen NA since we have implemented its source code while experimenting with other researches. We experiment in this section the results of NA after excluding the items which have not given a rate value greater than or equal to 1, 2, 3, or 4 by any user. We name the new algorithm after excluding items, NAO. We use the MovieLens (downloadable from [35]). MovieLens has 943 users and 1682 movies. It has 100,000 ratings, each from 1-5. Each user has rated at least 20 movies. In our experiments, we used the Visual Basic programming language [36], the Process Explorer Software to measure the CPU time, and 8-GB-RAM i7 PC.

TABLE I: THE NUMBER OF EXCLUDED ITEMS WHEN $minRate = 1, 2, 3, 4,$ and $5.$

minRate	Number of Excluded Items	(Number of Excluded Items)/ (Total Items) X 100%
1	0	0%
2	70	0.04%
3	108	0.06%
4	235	0.14%
5	510	0.3%

We split the items into two parts: training data and testing data. We used 80% of the items as training data. The remaining 20% of the items are used for testing. The 20% of the whole items are different for each users. To do so, we pass by every user, we choose randomly 20% of the items that he/she rated and we consider them as not rated.

We ran NA and NAO for 100 times for each user and we take the average of the 100 runs. We used the default parameters of the NA: mutation rate = 0.3, number of latent features = 6, number of generations = 200, crossover rate is equal to 0.8, population size = 50, $\alpha = 0.0002$, and $\beta = 0.02$. We calculated the Mean Absolute Error (MAE) in the same way as calculated by Navgaran et al. [18].

Table I presents the number of excluded items and the percentage of the excluded items to the total items when excluding the items which have not given any rate greater than ($minRate$) 1, 2, 3, 4, or 5. The percentage of the excluded items is equal to (number of excluded items)/(total number of items) X 100%. For instance, the number of excluded items and the percentage of the excluded items to the total items when $minRate = 3$ are 108 and 0.06 respectively. This means that there is no need to consider 108 items while searching for items to recommend to any active user since there is no any user gave any of these items a rate value of 3 or more. In other words, no any user gave a high rate to any of these items and hence NAO will not recommend any of these items to the active user. It is clear in Table I that the number of of excluded items and the percentage of the excluded items are increased as the $minRate$ increased. This happens since the number of items which has not given any rate greater than or equal to 1, 2, 3, 4 is less than the number of items which has not given any rate greater than or equal to 2, 3, 4, 5 respectively.

Tables II and III present the results of NAO and NA respectively. They show the average CPU time in seconds, MAE, accuracy, precision, and recall. In Table II, we excluded the results of NAO when $minRate = 5$ since it happens that many users will not have similar users and NAO cannot give recommendations for the users who has no other similar users.

It is clear from Table II that the average times in seconds taken are decreasing slightly when $minRate$ increased from 1 to 4. The MAE is decreasing as the $minRate$ increased. This happens since the number of items is decreased. The accuracy is increased as the $minRate$ increased since reducing the number of items reduces the search space and hence NAO needs to search fewer number of items as $minRate$ increased. There is a slight change in the precision as the $minRate$ increased. The recall is increased as $minRate$ increases from 1-3. After that the recall is decreased as $minRate$ is increased to 4.

Tables II and III show that the average CPU time taken by

TABLE II: THE RESULT OF RUNNING NAO.

minRate	Avg. Time(s)	MAE	Accuracy	Precision	Recall
1	2,775	2,866,456	0.6	0.67	0.8
2	2,679	2,825,625	0.64	0.6	0.93
3	2,685	2,805,111	0.73	0.71	0.96
4	2,652	2,794,745	0.87	0.7	0.87

TABLE III: THE RESULT OF RUNNING NA.

Avg. Time(s)	2,962
MAE	2,781,442
Accuracy	0.5
Precision	0.4
Recall	0.75

NA (2,962s) is greater than the average CPU time taken by NAO for any value of *minRate*. In addition, it shows that the accuracy, precision, and recall of NAO are better than of NA for any value of *minRate*. But, the MAE of NA is less than the MAE of NAO for any value of *minRate*. This happens since we have excluded some items and the MAE computed the actual difference between the actual rate and the expected rates.

VI. CONCLUSION AND FUTURE WORK

In this paper, we showed that if an item has not been rated high by any user, then no need to consider this item in the recommendation process. This reduces the time taken for the recommendation process and results in a better accuracy, precision, and recall values. We have proven this idea by incorporating it into Navgaran et al.'s algorithm [18] and testing it using the MovieLens dataset.

Nowadays, the RSs are overloaded with huge number of users and items. Therefore, further research is needed to reduce the number of items and users and to heuristically search for the recommended items in order to enable the RSs give recommendation in a short time.

ACKNOWLEDGMENT

Special thanks to my university, Hashemite University, for providing me the environment to do this research, department head, and my colleagues for their continuous encouragement.

Hashemite University supported us by a research grant to do this research.

REFERENCES

[1] J. Bobadilla, F. Ortega, A. Hernando, and J. Alcalá, "Improving collaborative filtering recommender system results and performance using genetic algorithms," *Journal of Knowledge-Based Systems*, vol. 24, 2011, pp. 1310–1316.

[2] P. Moradi and S. Ahmadian, "a reliability-based recommendation method to improve trust-aware recommender systems," *Journal of Expert Systems with Applications*, vol. 42(21), 2015, pp. 7386–7398.

[3] X. Yang, Y. Guo, Y. Liu, and H. Steck, "A survey of collaborative filtering based social recommender systems," *Journal of Computer Communications*, vol. 41, 2014, pp. 1–10.

[4] "http://www.netflix.com," 2018, URL: [accessed: 2018-10-11].

[5] "amazon," 2018, URL: http://www.amazon.com [accessed: 2018-10-11].

[6] "cdnow," 2018, URL: http://www.cdnnow.com [accessed: 2018-10-11].

[7] "drugstore," 2018, URL: http://www.drugstore.com [accessed: 2018-10-11].

[8] "drugstore," 2018, URL: http://www.eBay.com [accessed: 2018-10-11].

[9] R. Sikka, A. Dhankhar, and C. Rana, "A Survey Paper on E-Learning Recommender System," *International Journal of Computer Applications*, vol. 47(9), 2012, pp. 888–975.

[10] J. J. Castro-Sanchez, R. Miguel, D. Vallejo, and L. M. Lopez-Lopez, "A highly adaptive recommender system based on fuzzy logic for B2C e-commerce Portala," *Expert systems with applications*, vol. 38(3), 2011, pp. 2441–2454.

[11] S. Tan, J. Bu, C. Chen, and X. He, "Using rich social media information for music recommendation via hypergraph model," *ACM Transactions on Multimedia Computing, Communications, and Applications*, vol. 7(1), 2011, pp. 213–237, article 7.

[12] L. Duan, W. Sreat, and E. Xu, "Healthcare information systems: data mining methods in the creation of a clinical recommender system," *Enterprise Information Systems*, vol. 5(2), 2011, pp. 169–181.

[13] C. Porcel and E. Herrera-Viedma, "Dealing with incomplete information in a fuzzy linguistic recommender system to disseminate information in university digital libraries," *Journal of Knowledge-based Systems*, vol. 23(1), 2010., pp. 32–39.

[14] C. Porcel, A. Tejada-Lorente, M. Martinez, and E. Herrera-Viedma, "A hybrid recommender system for the selective dissemination of research resources in a technology transfer office," *Information Sciences*, vol. 184, 2012, pp. 1–19.

[15] "predictwallstreet," 2018, URL: http://www.predictwallstreet.com [accessed: 2018-10-11].

[16] E. V. Epure, B. Kille, J. E. Ingvaldsen, R. Deneckere, C. Salinesi, and S. Albayrak, "Recommending personalized news in short user sessions," *Proceedings of the Eleventh ACM Conference on Recommender Systems*, 2017, pp. 121–129.

[17] X. Guo and J. Lu, "Intelligent E-Government services with personalized recommendation techniques," *International Journal of Intelligent Systems*, vol. 22, 2007, pp. 401–417.

[18] D. Z. Navgaran, P. Moradi, and F. Akhlaghian, "Evolutionary based matrix factorization method for collaborative filtering systems," *Iranian Conference on Electrical Engineering*, 2013.

[19] N. E. I. Karabadj, S. Beldjoudi, H. Seridib, S. Aridhic, and W. Dhifli, "improving memory-based user collaborative filtering with evolutionary multi-objective optimization." *Expert Systems with Applications*, 2018, pp. 153–165.

[20] M. Volkovs, G. W. Yu, and T. Poutanen, "Content-based neighbor models for cold start in recommender systems," *11th ACM Conference on Recommender Systems*, 2017.

[21] S. B. CL1, C. Ramos, A. Rizo, and L. Fernandez-Luquecor, "HealthRecSys: a semantic content-based recommender system to complement health videos," *BMC Med Inform Decis Mak*, vol. 17(1):63, 2017.

[22] L. Safoury and A. Salah, "Exploiting User Demographic Attributes for Solving Cold-Start Problem in Recommender System," *Lecture Notes on Software Engineering*, vol. 1(3), 2013.

[23] H. R. Zhang, F. Min, X. He, and Y. Y. Xu, "A Hybrid Recommender System Based on User-Recommender Interaction," *Journal of Mathematical Problems in Engineering*, 2015, article ID 145636.

[24] S. Yanga, M. Korayemb, K. AlJadda, T. Grainger, and S. Natara-jana, "Combining content-based and collaborative filtering for job recommendation system: A cost-sensitive Statistical Relational Learning approach," *Journal of Knowledge-Based Systems*, vol. 136, 2017, pp. 37–45.

[25] Y. Kilani, A. Alsarhan, M. Bsoul, and S. El-Salhi, "Local search-based recommender system for computing the similarity matrix," *Int. Journal of Intelligent Systems Technologies and Applications*, 2018, forthcoming.

[26] Q. Shambour and J. Lu, "A hybrid multi-criteria semantic-enhanced collaborative filtering approach for personalized recommendations," *Proceedings of the International Conferences on Web Intelligence and Intelligent Agent Technology (WI-IAT)*, 2011, pp. 71–78.

[27] B. Jadoon, A. Mansha, F. H. Khan, and S. Bashir, "collaborative filtering based online recommendation systems: a survey," *International Conference on Information & Communication Technologies*, 2017.

[28] C. C. Aggarwal, "recommender systems: chapter 2," *Springer International Publishing Switzerland*, 2016.

- [29] D. Bokde, S. Girase, and D. Mukhopadhyay, "Matrix Factorization Model in Collaborative Filtering Algorithms: A survey ," *Procedia Computer Science*, vol. 49, 2015, pp. 136–146.
- [30] Z. Lu, Z. Dou, J. Lian, X. Xie, and Q. Yang, "content-based collaborative filtering for news topic recommendation ," *Proceedings of the Twenty-Ninth AAAI Conference on Artificial Intelligence*, 2015, pp. 217–223.
- [31] P. Lops, M. De Gemmis, and G. Semeraro, "Content-based recommender systems: state of the art and trends," *Recommender systems handbook*, 2011, pp. 73–105.
- [32] R. Boim and T. Milo, "Methods for boosting recommender systems," *2011 IEEE 27th International Conference on Data Engineering Workshops*, 2011.
- [33] Y. Bachrach, Y. Finkelstein, and R. BachrachRan, "Speeding up the xbox recommender system using a euclidean transformation for inner-product spaces," *Proceedings of the 8th ACM Conference on Recommender systems*, 2014, pp. 257–264.
- [34] V. Formoso, D. Fernandez, F. Cacheda, and V. Carneiro, "Using rating matrix compression techniques to speed up collaborative recommendations," *Journal of Information Retrieval*, vol. 16(6), 2013, pp. 680–696.
- [35] "MovieLens," 2018, URL: <http://grouplens.org/datasets/movielens/> [accessed:2018-10-11].
- [36] J. Foxall, "Visual Basic 2015 in 24 Hours," Sams Publishing, vol. 1st edition, 2016.

CLINIC: A Web Healthcare Management System for Enhancing Clinical Services

Ahmad R. Qawasmeh, Dema Awni, Raghad Mohammed, Rufaida Sabri, Ghydaa Ahmad

Department of Computer Science
The Hashemite University
Zarqa, Jordan

Email: ahmadr@hu.edu.jo, Owais.dema96@gmail.com, raghad-aboawais@bayt.net,
rufaida.sabri@yahoo.com, ghydaaah22@yahoo.com

Abstract—Clinic systems have become widely used nowadays by everyone involved in the medical field. These systems can be either desktop applications, Web applications, or even mobile applications. However, most of the currently available systems are either limited to one clinic, hospital or organization, restricted in terms of usability, hard to maintain and modify, or lacking important communication features. In this work, we propose an open-source medical Web application called CLINIC targeting patients and clinicians worldwide. CLINIC allows clinicians to register upon identity verification. It enhances patient-clinician communication and provides new useful services that include, but are not limited to secure registration by patients and doctors, secure storage of patients' records, instant chatting for consultation, helpful medical articles and first aid tips, and user-friendly interface. CLINIC has good potential to become widely used because of its new features, services, and ambitions.

Keywords—Clinic system; Performance analysis and improvement; Patients monitoring; Healthcare management system.

I. INTRODUCTION

Clinic systems have been growing rapidly in the last few decades to provide better healthcare for patients via reliable computer-based applications. Clinic systems are responsible for the management of a healthcare facility while meeting the high standards of security, functionality and technology that must be associated with patients' medical records.

According to [1], a healthcare system contains four nested levels: (1) the patient; (2) the care team (e.g., physicians, pharmacists, family members, etc); (3) the organization (e.g., clinic, hospital, etc.); and (4) the political and economic environment (e.g., regulations, financial payment methods). Any computerized healthcare system should adapt to the aforementioned levels in one way or another.

Due to the massive growth of modern computer-based methods, it has become much easier to simplify the difficulty of maintaining patients' manual records by computerizing them. This computerization process has many advantages that include efficient patient data retrieval and sharing, secure data protection, confidential accessing, better clinic productivity, and low management costs while reducing human errors. While a clinic system can be developed as a desktop application or mobile application, Web applications can provide better features with more convenient access. In terms of desktop applications, they have to be installed separately on each computer while also having a usability constraint depending on the physical location where they are installed. On the other hand, mobile applications overcome the aforementioned desktop constraints, but convenient usability remains a big issue especially when

it comes to clinic systems where management is the main concern.

In this work, we propose an open-source Web healthcare application (CLINIC) that provides various features and services commonly used and required in clinic systems. The application offers a suitable environment for users (clinicians, nurses, patients, and administrators), who are involved in the healthcare process. Our application provides an interactive way for communication between clinicians, nurses and patients, while maintaining high standards of security and functionality. CLINIC offers a variety of services to any clinician who needs a reliable management system to his/her clinic.

The main motivation of this work lies in the following points:

- Clinicians need to have an interactive system that allows them to manage and access the records of their patients conveniently regardless of location or any other constraints especially in the case of emergency.
- Patients need a user-friendly system that allows them to check the status of their cases, schedule a new appointment, get information about clinicians, and check the orders of their pharmacy medications and labs while saving cost, time and effort.
- Requesting a consultancy through common websites may take so long. This makes online chatting very useful and even necessary in urgent cases.
- Maintenance, usability, security, cost and performance are critical factors that must be handled efficiently by any clinic system.

This paper is organized as follows. Section 2 discusses the related work. Section 3 describes the methodology, implementation, and Graphical User Interface (GUI) of the proposed system. Finally, Section 4 concludes our contributions and mentions directions for the future work.

II. RELATED WORK

Different desktop, Web and mobile applications have been developed to facilitate the process of healthcare all around the world. These applications vary in terms of efficiency, usability, reliability, and security. In this section, we tried to cover the most recent and relevant clinic systems.

Hakeem [2] is a program that was developed to automate the public healthcare sector in Jordan. Hakeem aims to provide high-quality healthcare in Jordan via the implementation of an Electronic Health Record (EHR) solution. Hakeem provides

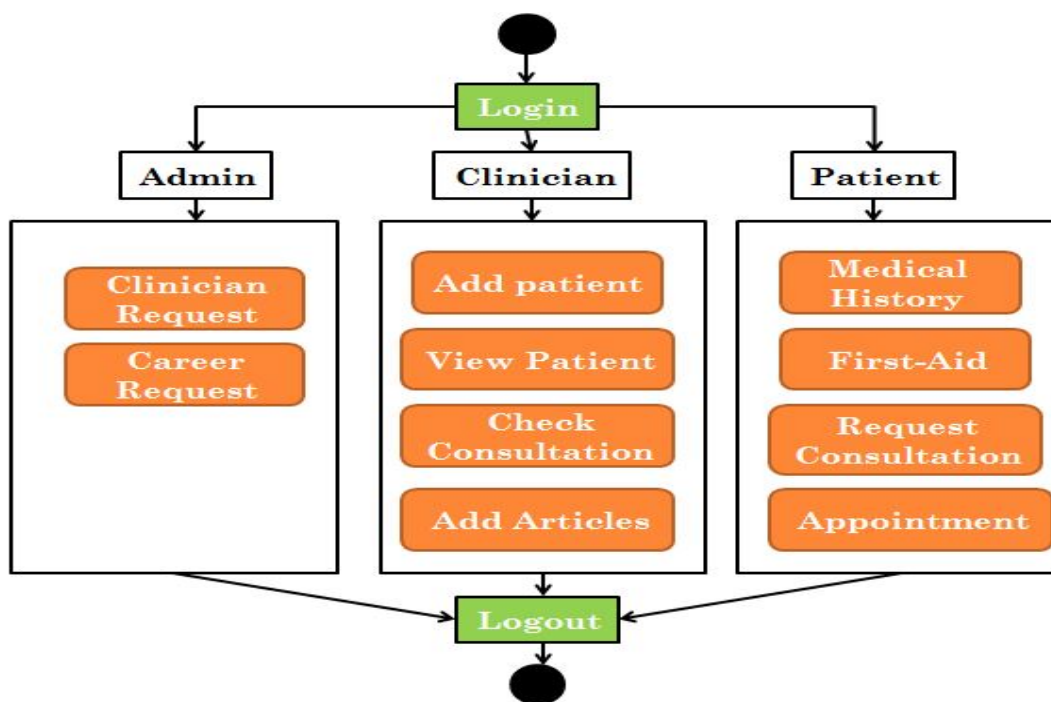


Figure 1. Main components of CLINIC

online access to medical history examinations, lab results, clinic visit notes, etc. Clinicians can electronically access medical records of patients by simply entering the patients national ID number. While Hakeem facilitates the process of healthcare, it lacks patients' involvement and access to their records. Altibbi [3] is a website that focuses on medical consultancy. This website has more than 10000 registered clinicians, who respond to patients queries in short time. It also shows recent medical articles and news. However, consultancy is not for free. OpenClinic GA [4] is an open-source Hospital management Information System (HIS) that has been used in more than 500 hospitals and clinics in many countries. OpenClinic provides many healthcare modules that include patient administration, financial management, medical records and imaging, among others. E-HAS [5] is an online-offline HIS for Healthcare organizations. It provides various paid features and modules. Medical Digital-Ray (MDR) free system [6] is a healthcare system created to enhance the efficiency of medical and administrative processes of small hospitals and clinics.

AMD [7] is an eye-specialized program that offers simulation of Age-related Macular Degeneration (AMD), which captures both the detailed operation of an eye clinic and the broader social care of AMD sufferers.

There are other light-weight systems [8]–[11] that can be used to maintain the records of patients in small clinics.

In contrast with the aforementioned apps, our application is a free-access system that allows patients to get involved in the healthcare process, while offering various beneficial management, administrative and communication features.

In terms of mobile applications, there are many apps, which can be installed on both IOS and Android systems. Epocrates [12] is being used by doctors to search for drug info, find other providers for consults and calculate beneficial measurements.

Doximity [13] is the largest medical professional network in the U.S used for communication, reading medical news, and career management. Medscape [14] is another app that can be used to look up medications and drugs, check medical news, and more. As can be figured out, mobile apps are not designed for clinic systems. However, they are beneficial in terms of measurements and medical news.

There are other applications that have been developed and used in the context of clinic systems. However, we tried to focus on the most recent and relevant ones.

III. METHODOLOGY AND IMPLEMENTATION

As design is so important in any Web application, we tried to develop an attractive graphical interface that provides convenient way of interaction for clinicians/patients. In other words, user can easily register in our application and choose the required action depending on his/her permissions. Our system responds by displaying the wanted information in a user-friendly manner. Figure 1 shows the main components of our proposed system.

In our application, we used Hyper Text Markup Language (HTML), Cascade Style Sheet (CSS) and Java-script to design the front-end environment, while using Personal Home Page (PHP) for implementing the back-end functions and methods. We also used MySQL to create our database, which consists of 13 tables while taking into account the cardinality and relationships among them.

A. User Interface

The home page of our application, shown in Figure 2, contains four tabs reachable easily by the user. By clicking on the "Doctors" tab, all registered clinicians will be displayed. By clicking on the "Join us" tab, Figure 3 will be displayed.

This figure contains two clickable images; one for clinicians and the other for patients. Once the clinician clicks on his image, he will be transferred to the page shown in Figure 4.



Figure 2. Home page

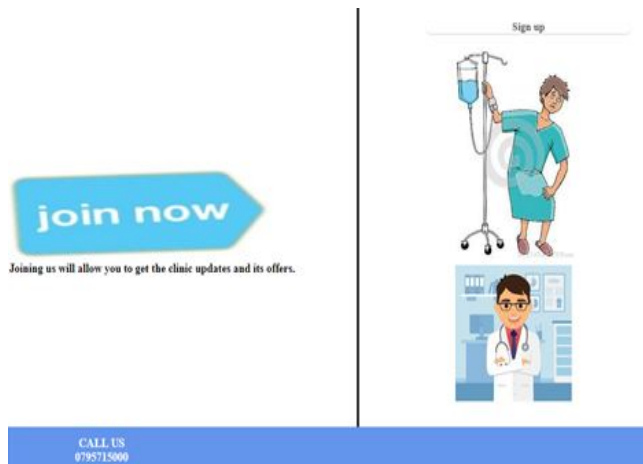


Figure 3. Join us page



Figure 4. Signup page with captcha

The clinician needs then to enter his doctor's syndicate ID,

password and captcha letters and click on the Signup button. A request will be sent to the admin page shown in Figure 5. The admin must verify the identity of the clinician by contacting the doctor's syndicate. Once the verification process is done, the admin allows the clinician to use the application with all its features. The front-desk staff of any clinician can help any patient to register in the application via his/her SSN. Once the patient registers, his credentials will be saved in the system to be used for any future visits. The last tab in the home page is "Careers", where any clinician can attach his information and resume without the need for registration for future consideration. The career page is shown in Figure 6.



Figure 5. Admin main page



Figure 6. Career request page

The clinician page, shown in Figure 7, has different activities. The clinician can add a medical record to any patient upon treatment completion, as shown in Figure 8. The Orders textbox can be one or more of pharmacy medications, labs (e.g., Complete Blood Count CBS, Blood group, Kidney Function Test, etc), radiology (e.g., X-Ray or Ultrasound), and/or Nursing (e.g., injections, nebulizer, wound change, etc). The clinician can also add an article, view his/her patient(s) medical history as shown in Figure 7, and check any online consultation requested from him. A clinician can display his/her patients records only. The clinician can view either all his/her patients'



Figure 7. Clinician main page



Figure 9. Patient main page



Figure 8. Add patient's record page

records, a specific patient's record based on a specific SSN, or patients' records in a specific date.

Patient's page is shown in Figure 9. Patient can check his/her medical history by entering SSN. Each visit to any clinician registered in CLINIC will be displayed with all the details including date, orders, clinician name and address, disease, and any comments from the corresponding clinician. Patient can also check some updated medical articles, as shown in Figure 10, and view some useful first aid tips. Last but not least, patient can request an online chatting consultation, as shown in Figure 11. This online chatting is based on instant messages sent from patients to available clinicians and vice versa.

New healthcare features and activities can easily be added to our application. The appointment scheduling module should be added soon to make the application even more powerful and reliable.

IV. CONCLUSIONS AND FUTURE WORK

In this paper, we proposed a Web-based application called CLINIC. CLINIC was designed as an open-source clinic

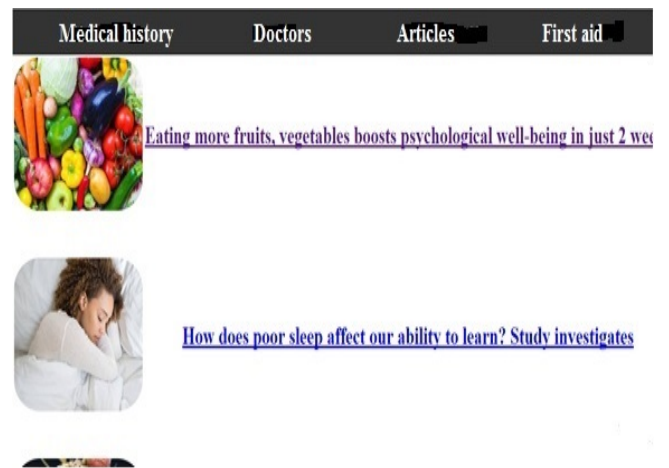


Figure 10. Medical articles page

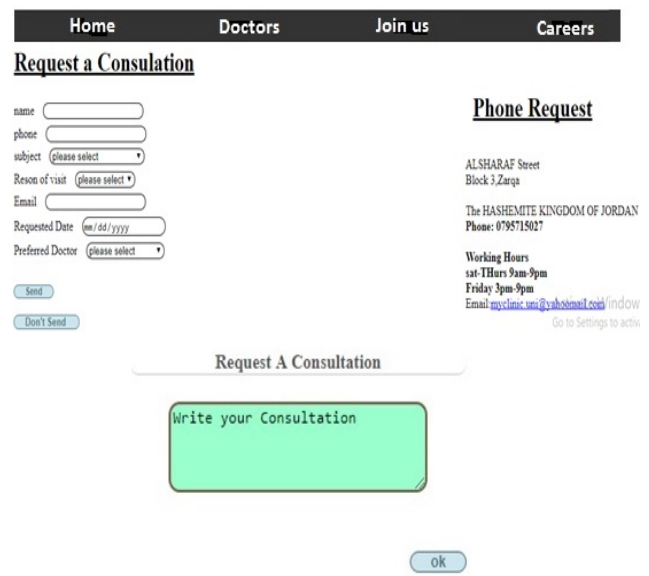


Figure 11. Request consultation page

system that can be used by patients/clinicians to facilitate the process of healthcare management and administration. CLINIC provides a free-access interactive environment and meets the high-quality requirements of security, technology and functionality. CLINIC comprises different modules that cover many useful features and activities for both clinicians and patients. CLINIC allows clinicians to manage and access the records of their patients conveniently. It also authorizes patients to check the status of their cases, get information about clinicians, request online instant consultation, and check the orders of their pharmacy medications and labs while saving cost, time and effort. Last but not least, CLINIC demonstrated promising results and hence it has the capability to be used on a larger scale.

Path forward, we plan to integrate more modules such as appointment scheduling into CLINIC. We also think that making this app available on mobile phones should positively affect its popularity.

ACKNOWLEDGMENT

The authors would like to thank the Hashemite University for providing the required resources.

V. REFERENCES

- [1] E. B. Ferlie and S. M. Shortell, "Improving the quality of health care in the united kingdom and the united states: A framework for change," *The Milbank Quarterly*, vol. 79, no. 2, pp. 281–315, 2001.
- [2] Sprintive, *EHS Electronic Health Solutions Technology for better healthcare in Jordan*, <https://ehs.com.jo/hakeem-program>, Accessed: 10-09-2018, 2018.
- [3] Altibbi, *altibbi*, <https://www.altibbi.com/>, Accessed: 10-09-2018, 2016.
- [4] frankverbeke, *OpenClinic GA*, <https://sourceforge.net/projects/open-clinic/>, Accessed: 10-09-2018, 2018.
- [5] techdynamics, *Hospital Management System Enterprise*, <https://sourceforge.net/projects/enterrpise-hospital-system/>, Accessed: 10-09-2018, 2018.
- [6] digitalray, *MDR Clinics - polyclinic system*, <https://sourceforge.net/projects/medical-digital-ray/>, Accessed: 10-09-2018, 2018.
- [7] sprossiter, *AMD-HealthSocialCareSim*, <https://sourceforge.net/projects/amdhealthsocialcaresim/>, Accessed: 10-09-2018, 2018.
- [8] nasir031, *Homeo Medica*, <https://sourceforge.net/projects/homeomedical/>, Accessed: 08-09-2018, 2018.
- [9] abolkog, *zClinic*, <https://sourceforge.net/projects/zclinic/>, Accessed: 09-09-2018, 2018.
- [10] macdonaldgeek, *OpenPatientOS*, <https://sourceforge.net/projects/patientosremade/>, Accessed: 07-09-2018, 2018.
- [11] congvan, *Patient Management System*, <https://sourceforge.net/projects/patientms/>, Accessed: 07-09-2018, 2018.
- [12] Epocrates, *Epocrates*, <https://itunes.apple.com/us/app/epocrates/id281935788?mt=8>, Accessed: 06-09-2018, 2018.
- [13] Doximity Inc, *Doximity - Medical Network*, <https://play.google.com/store/apps/details?id=com.doximity.doximitydroid&hl=en>, Accessed: 06-09-2018, 2018.
- [14] WebMD, *Medscape*, <https://itunes.apple.com/us/app/medscape/id321367289?mt=8>, Accessed: 06-09-2018, 2018.